# Role of the obligate STRIPAK complex component Mob4 in zebrafish vascular development and stability

Tvisha Misra[1-3], Shimon M. Rosenthal[2-4], Mengyi Song[5,6], Nathan J. Stutt[2,3], Laura McDonald[2,3], Ashish R. Deshwar[2,3,7,8], Anne-Claude Gingras[2,4], Ian C. Scott[2,3]

1. Department of Urology, University Hospital Essen, Germany
2. Department of Molecular Genetics, University of Toronto, Toronto, Canada
3. Program in Developmental and Stem Cell Biology, The Hospital for Sick Children, Toronto, Canada
4. Lunenfeld-Tanenbaum Research Institute, Mount Sinai Hospital, Sinai Health, Toronto, Canada
5. The Eli and Edythe Broad Center of Regeneration Medicine and Stem Cell Research, University of California San Francisco, San Francisco, USA
6. Department of Neurology, University of California San Francisco, San Francisco, USA
7. Division of Clinical and Metabolic Genetics, The Hospital for Sick Children
8. Department of Paediatrics, University of Toronto

## Abstract

The **STR**iatin **I**nteracting **P**hosphatases and **K**inases (STRIPAK) complex is a conserved multiprotein module with functions in cell proliferation, cell growth, and cancer. Primarily examined through proteomic and *in vitro* studies, there is a relative lack of insight into the *in vivo* function of the STRIPAK complex during development. Motivated by the prominent interaction of STRIPAK and the CCM3 adapter protein, which is associated with the vascular disease cerebral cavernous malformation (CCM), we sought to examine the role of the conserved STRIPAK component Mob4 in early zebrafish vascular development. We use proximity-dependent biotinylation (BioID) coupled with mass spectrometry to show that Mob4 is a component of the STRIPAK complex in zebrafish. Loss of *mob4* leads to pronounced cardiovascular and neuronal defects, including a leaky cerebral vasculature, hypersprouting of venous endothelial cells and poor neuronal branching. Conditional transgenic models further demonstrate a continuous and broad requirement for Mob4 in development. Taken together, these results suggest a key role for STRIPAK function in vascular development and stability, replicating hallmarks of CCM.

# Introduction

The coordination of signalling pathways is a key process during development and physiological homeostasis whose deregulation has been linked to a variety of conditions, including vascular diseases. Multiple signalling events are mediated through scaffolded protein complexes, which are thought to provide specificity to substrate selection and spatio-temporal control of the signalling events. The Striatin-interacting phosphatase and kinase (STRIPAK) complexes are large, highly conserved multiprotein structures scaffolded by the large Striatin proteins (Castets et al., 1996; Goudreault et al., 2009). Striatin orthologs and multiple STRIPAK components are conserved through evolution (three in mouse and humans, and one each in *D. melanogaster* and *C. elegans* (Hwang and Pallas, 2014). In mammals, paralogous expansion and mutually exclusive interactions among STRIPAK components give rise to multiple distinct assemblies, although the specific functions of these complexes remain incompletely understood. As its name suggests, the STRIPAK complex contains both phosphatases (the PP2A phosphatase catalytic and scaffolding subunit, the latter of which directly binds to Striatin) as well as kinases (the GCK-III family of Sterile-20 kinases that are recruited to the STRIPAK scaffold via the adapter protein CCM3/PDCD10) (Kean et al., 2011; Moreno et al., 2000). STRIPAK also associates with other kinases to modulate various signalling pathways, including the Hippo pathway (Couzens et al., 2013; Ribeiro et al., 2010). Consistent with these roles, dysregulation of Striatin family members and their interactors has been implicated in human disease, particularly in cancer cell migration and metastasis (Bisoyi et al., 2022; Hwang and Pallas, 2014; Kim et al., 2020; Kück et al., 2016; Madsen et al., 2015; Qiu et al., 2020; Shi et al., 2016; Tang et al., 2020).

Striatins are important for various processes such as dendrite outgrowth, hearing development, dorsal closure, excretory canal formation, sarcomere formation, and neuronal development (Bartoli et al., 1998; Berger et al., 2022; Lahav-Ariel et al., 2019; Lant et al., 2015; Li et al., 2018; Nadar-Ponniah et al., 2020). Given the cell-type-specific expression and potentially redundant or specialized roles of Striatin paralogs, further work is needed to assess the developmental roles of the STRIPAK complex. Among the many STRIPAK components is MOB4 (formerly known as Mob3 or Phocein;(Baillat et al., 2001)), a member of the evolutionarily conserved monopolar spindle-one-binder family best known for its role as a kinase regulator. The presence of multiple paralogs for most STRIPAK components in vertebrates complicates comprehensive functional analyses of the complex. However, MOB4 is consistently identified as a core STRIPAK component in multiple vertebrate species (Baillat et al., 2001; Goudreault et al., 2009; Jeong et al., 2021) and human MOB4 is able to functionally replace its *Drosophila* counterpart (Schulte et al., 2010). Rat Mob4 is enriched in brain tissue in dendritic and Purkinje cells and to a lesser extent in several other tissues

(Baillat et al., 2001; Bailly and Castets, 2007; Castets et al., 1996; Haeberlé et al., 2006). In *Drosophila* S2 cells, Mob4 localizes to mitotic centres and kinetochores and regulates spindle organization in mitotic cells (Trammell et al., 2008). Loss of Mob4 leads to defects in spermatid differentiation (Santos et al., 2023), axonal transport, and microtubule organisation (Schulte et al., 2010; Sepp et al., 2008). In *C. elegans*, *mob-4* is widely expressed, with loss leading to reduced lifespan and thermotolerance (Jahan et al., 2021). In planarians, Mob4 knockdown loss leads to increased body size and defects in proportionality and tissue rescaling during regeneration (Schad and Petersen, 2020). In zebrafish, Mob4 is localized to Z discs in the sarcomere and is required for sarcomere organization, with further roles in neuronal and cartilage development, cell survival and organization of microtubule networks (Berger et al., 2022). Despite these insights, a comprehensive analysis of MOB4 and STRIPAK function during early vertebrate development remains lacking.

Here, we describe the role of Mob4 in early zebrafish development. Using proximity-dependent biotinylation, we define the *in vivo* interactome of Mob4, which closely parallels previously reported *in vitro* data from mammalian systems, confirming its role as a core STRIPAK component. Analysis of a *mob4* mutant model reveals defects in cardiac, vascular and neuronal development. In the vasculature, Mob4 loss leads to defects in blood vessel integrity and endothelial cell migration, specifically in venous endothelial cells. We show that *mob4* mutant defects can be rescued by ubiquitous expression of a Mob4 transgene and find that Mob4 is required continuously for proper vascular development. Via restoration of Mob4 function, we show that *mob4* phenotypes can be partially rescued by re-expression of Mob4. Taken together, these results indicate broad and continuous requirements for STRIPAK/Mob4 in vertebrate development and suggest a critical role for the STRIPAK complex in vascular development and stability.

# Results

## Mob4 is a primary component of the STRIPAK complex in zebrafish

To define the *in vivo* interactome Mob4, we used a biotin-dependent proximity labelling approach employing the biotin ligase TurboID (Branon et al., 2018) in zebrafish embryos (Rosenthal et al., 2021) (Fig 1A). We injected one-cell stage embryos with mRNA encoding Mob4, N-terminally tagged with TurboID and C-terminally tagged with EGFP (TurboMob4EGFP). TurboEGFP RNA and uninjected embryos were used as controls. Embryos were incubated in biotin-supplemented egg water from 12 to 48 hours post-fertilization (hpf), followed by protein purification and mass spectrometry analysis (Rosenthal et al., 2021). Data from 2 replicates of *TurboMob4EGFP* were compared against multiple

replicates of *TurboEGFP* and uninjected controls using the SAINTexpress software (Teo et al., 2014). Proteins with a Bayesian false discovery rate (BFDR) ≤5% are considered high-confidence proximity partners (a complete list of proximal interactors and their human orthologs is provided in Supplementary Tables S1 and S2). As expected, the top enriched hits largely comprised components of the STRIPAK complex, including Striatin/Striatin3/Striatin4, Slmap, Fam40a/Strip1, and Cttnbp2/Cttnbp2L (Fig 1B). Gene Ontology (GO) gene set enrichment analysis of the human orthologs of high-confidence hits showed the "STRIPAK complex" as the most significantly enriched GO term (Fig 1C, and Supplementary Tables S3). The *in vivo* Mob4 interactome therefore strongly suggests a conserved role for Mob4 in STRIPAK complex function during zebrafish embryogenesis.

## *mob4* loss leads to early cardiovascular defects

To investigate the role of Mob4 in development, we generated a *mob4* mutant model via injection of CRISPR/Cas9 ribonucleoprotein (RNP) complexes targeting exon 3 (Fig 2A, red circle). An allele with an 11 base pair deletion was isolated (Fig 2B, top panel *mob4 mutant*), leading to a premature STOP codon early in the kinase regulation domain (Fig 2A). *mob4* mutant embryos exhibited cardiac oedemas at 56 hpf (Fig 2C', black arrowhead), indicating early cardiovascular defects. We use double transgenic *kdrl:EGFP*; *gata1:dsRed* embryos to visualize endothelial cells (ECs) with EGFP and red blood cells with dsRed. In contrast to wild-type embryos, in *mob4* mutant embryos, blood flow was lost over time, as evidenced by stationary blood cells in the tail trunk (Fig 2D and D', white arrowhead). Additionally, *mob4* mutant embryos exhibited instances of cranial haemorrhaging (Fig 2D', yellow arrowhead) as seen by aggregation of dsRed-positive blood cells in the hindbrain. The severity of both cardiac oedemas and cranial haemorrhages in *mob4* mutant embryos at 72 hpf varied (Fig 2E-E'''', magenta and blue asterisks, respectively). Haemorrhages were not observed in the tail trunk vasculature, suggesting a vascular bed-restricted role for Mob4.

Given the cardiac oedemas and progressive loss of blood flow in *mob4* mutant embryos, we next examined cardiac development via the use of *kdrl:mApple; myl7:EGFP* transgenic embryos, in which the endothelium and endocardium are labelled with mApple and the myocardium is labelled with EGFP (Fig 2F-H'''). While atrial and ventricular chambers and a patent outflow tract with an endocardial lining were apparent in *mob4* mutants at 72 hpf, in many cases, heart looping and morphogenesis of the atrioventricular canal were abnormal (Fig 2H-H''', orange asterisks). Large oedemas were apparent in the majority of *mob4* mutant embryos (Fig 2H-H''', white arrowheads), which may contribute to defects in cardiac development. Overall, overt defects in cardiac and vascular development were apparent in *mob4* mutants.

137 ***mob4* mutants exhibit defects in cerebral vasculature**

138 Given the cerebral haemorrhaging observed in *mob4* mutants, we next examined the
139 development of the cranial vasculature. At 48 hpf, the overall architecture of the vasculature
140 was not affected in *mob4* mutants, with major vessels and structures such as the dorsal
141 midline junction (DMJ) easily identifiable (Fig 3A-B''). Haemorrhages could be readily
142 identified by the accumulation of blood cells outside the vasculature at 48 hpf (Fig 3B-B'',
143 yellow arrowhead. By 96 hpf, vascular defects were more pronounced in *mob4* mutants (Fig
144 3C-D''). Blood flow was largely halted, as evidenced by stationary blood cells. Further,
145 collapsed vessels were evident such as the Dorsal Longitudinal Vein and Dorsal Midline
146 Junction (Fig 3D'', asterisks). We next used time-lapse imaging to track the development of
147 cerebral haemorrhages and cessation of blood flow in *mob4* mutants starting at 54 hpf in the
148 *kdrl:EGFP*; *gata1:dsRed* double transgenic background. Fig 3E-F shows projections of z-
149 stacks of single time points from imaging over 54 to 72 hpf (Supplementary movie 1).
150 Angiogenesis could be observed in the extension of ECs to establish new central arteries
151 (Fig 3E, asterisks), which subsequently lumenized and established blood flow. Early cerebral
152 blood flow was established in *mob4* mutant embryos (Fig 3F-F'''). However, in some cases
153 (arrowheads Fig 3F'''-F'''') after a nascent vessel was lumenized and blood flow established,
154 a haemorrhaging event occurred with blood leakage. Blood vessels continued to experience
155 blood flow after haemorrhage events. Similar time-lapse imaging was carried out on the tail
156 trunk vasculature, beginning at 54 hpf when vessels were lumenized and robust blood flow
157 could be observed in not only the larger dorsal artery (DA) and caudal venous plexus (CVP)
158 but also the smaller intersegmental vessels (ISVs) (Supplementary movie 2). The extent of
159 tail trunk blood flow in *mob4* mutant embryos at 54 hpf varied broadly, with either robust flow
160 at 54 hpf or a relative absence of blood cells and flow from as early as 54 hpf (Fig 3G-I). In
161 *the mob4* mutant embryos, blood flow was established in early development, similarly to
162 control embryos, but was gradually lost over time, though the exact developmental stage at
163 which this happened varied between embryos. Independent of the degree of blood flow,
164 *mob4* mutants exhibited aberrant sprouting of trunk blood vessels, which arose from either
165 ISVs (red asterisks) or the ventral vascular bed (blue asterisks) (Fig 3G-I), with aberrant
166 vascular sprouting occurring in a manner seemingly independent of loss of flow in affected
167 vessels (Fig 3I). Defects were evident in retinal vasculature as well (Fig 3J-J'').

168 The blood vessel comprises the inner endothelial layer composed of ECs and surrounding
169 supporting architecture consisting of basal, lamina pericytes and astrocytes (Gaengel et al.,
170 2009). Defects in pericyte localization and function lead to vascular instability and
171 haemorrhaging (Rajan et al., 2020). We found that pericyte localization (as indicated by use
172 of a *pdgfrb:Citrine* transgenic line (Ando et al., 2016; Vanhollebeke et al., 2015) was not

173 obviously affected in *mob4* mutant embryos compared to *control* embryos (Fig S1); with both
174 head and tail trunk vasculature comparably decorated with pericytes. Overall, while the
175 development of the cerebral vasculature was initiated normally in *mob4* mutants, there was
176 a subsequent failure in vascular integrity prior to a loss of blood flow. While leakage was not
177 observed in the tail trunk vasculature, abnormal angiogenesis did similarly result from the
178 loss of Mob4.

## 179 *mob4* mutants exhibit hypersprouting of venous endothelial cells in the tail 180 trunk

181 We next examined the nature of tail trunk EC hypersprouting in *mob4* mutant embryos.
182 Primary angiogenic sprouting of ECs from the dorsal aorta (DA) along the myotome
183 boundaries occurs from 20-36 hpf. Subsequently, during secondary angiogenesis, venous
184 ECs from the posterior cardinal vein (PCV) migrate along the same myotome boundaries
185 from 36-60 hpf. The intersegmental vessels thus formed are only functionally determined as
186 arterial or venous depending on the interaction of the newly formed secondary vessels with
187 the previously established primary network (Isogai et al., 2003). As our initial analysis of
188 *mob4* mutants suggested defects in secondary angiogenesis (Fig 3H-I'''), we used the Notch
189 reporter line *tp1:EGFP* to label arterial ECs (Quillien et al., 2014). In double transgenic
190 *tp1:GFP*; *kdrl:hRasmCherry* embryos all ECs are labelled with membrane-targeted mCherry
191 and arterial ECs are labelled with GFP (Fig 4 A-C''). In *mob4* mutant embryos, hypersprouting
192 ECs (Fig 4 B', C', yellow asterisks) were labelled with mCherry but negative for EGFP,
193 suggesting a non-arterial nature. Time-lapse imaging of embryos from 56-71 hpf was carried
194 out to visualise EC hypersprouting in real time. Representative wild type and *mob4* mutant
195 embryos are shown in Supplementary movie 3. As expected, hypersprouting was already
196 evident in some *mob4* mutant embryos at 56 hpf (Supplementary movie 3C-C'' white
197 asterisks); however, subsequent *de novo* hypersprouting events were also observed
198 (Supplementary movie 3B-B'', yellow asterisks). Hypersprouting ECs were all negative for
199 EGFP. We further used a *mrc1a:GFP* transgenic line to mark venous and lymphatic ECs,
200 (Fig 4 D-D'') (Jung et al., 2017). In *mob4(-/-)*; *kdrl:hRasmCherry*; *mrc1a:EGFP* embryos, all
201 hypersprouting ECs in the tail trunk were labelled with both EGFP and mCherry. Thus, our
202 data strongly suggest that hypersprouting ECs do not arise during the primary angiogenic
203 wave but are instead venous in origin.

204 We next asked if the hypersprouting EC phenotype can be rescued by the expression of
205 Mob4 in venous ECs. *Lyve1* is a highly specific marker of lymphatic cells, although it is also
206 active in a subpopulation of venous endothelial cells. Zebrafish *lyve1* expression is observed
207 in both lymphatic and venous vascular structures such as the caudal vein, common cardinal

208 vein, and the posterior cardinal vein (Okuda et al., 2012) (Fig 4G-G''). Strikingly in *mob4(-/-)*; *kdrl:hRasmCherry*; *lyve1:Mob4EGFP* embryos, there were no discernible instances of
209
210 hypersprouting blood vessels and vessels of the tail trunk were comparable to those of
211 control embryos (Fig 4G-I''). Thus, we conclude that *lyve1* promoter-driven *mob4* re-
212 expression results in rescue of hypersprouting of venous/lymphatic ECs from the caudal
213 venous plexus. This indicated a cell-autonomous role for Mob4 in venous/lymphatic ECs
214 during the secondary angiogenic phase of vascular development.

## 215 *mob4* mutants exhibit neuronal branching defects

216 Given the role of many STRIPAK complex members in neuronal development and function,
217 we next examined the developing nervous system in *mob4* mutant embryos. Using a pan-
218 neuronal *Tg[ngnl:mKate]* (Kinney et al., 2020) line to image neurons, we first examined *mob4*
219 mutants at 84 hpf. Both impaired arrangement of cranial neuronal bundles and reduced
220 sprouting of tail trunk motor neurons were consistently observed (Fig 5A-B''). To further
221 examine the nature of neuronal defects, time-lapse imaging was employed from 54 hpf, when
222 motor neuron migration from the spinal cord is initiated (Myers, 1985; Myers et al., 1986). In
223 *mob4 mutant* embryos, initial motor neuron migration/outgrowth at 54 hpf was impaired (Fig
224 5D-D'', blue and yellow asterisk) compared to wild type (Fig 5C-C''). Primary outgrowth of
225 motor neurons is followed by secondary and tertiary outgrowth (Fig 5C''-C''', red, green and
226 purple asterisks follow single motor neurons). In contrast, in *mob4* mutants, various instances
227 of migration defects were observed: impaired (yellow asterisk) or no (blue asterisk)
228 secondary migration, looping of axonal outgrowths (brown asterisk) or short non-elongating
229 outgrowths (yellow asterisk) (Fig 5D-D''). These results show that complete Mob4 loss leads
230 to severe defects in the development of the nervous system.

## 231 Continuous requirement of Mob4 function during development and adult
## 232 physiology

233 Our analyses indicated a number of cell types affected by Mob4 loss. To further examine
234 cell-autonomous functions of Mob4, we generated a conditional rescue transgenic line (*Tg*
235 *ubi:loxP-mScarletNLS-loxP-TurboMob4EGFP*) in which Mob4 expression can be activated
236 via temporal- or tissue-specific Cre activity (Fig S2A). A *hsp70l:Cre* transgenic line (Pan et
237 al., 2011) was used to induce rescue transgene expression via dual heat shock at 24 and 30
238 hpf. While wild-type transgenic embryos appeared normal at 120 hpf (Fig S2C-D), all *mob4*
239 (-/-); *ubi:loxP-mScarletNLS-loxP-TurboMob4EGFP; hsp70l:Cre* embryos without heat shock
240 demonstrated expected phenotypes including cardiac, ocular and brain oedemas, small
241 eyes, defects in body shape and improper fin development (Fig S2E-E'). This indicated
242 minimal leakiness of the rescue transgene. In contrast, *mob4* (-/-); *ubi:loxP-mScarletNLS-*

243 *loxP-TurboMob4EGFP; hsp70l:Cre* embryos treated with double heat shock showed
244 consistent rescue of phenotypes at 120 hpf in 4/5 embryos, with 1/5 embryos exhibiting a
245 curved body axis (Fig S2 F-F'). These results correspond to previous studies showing
246 ubiquitous expression of Mob4 to rescue loss-of-function defects (Schulte et al., 2010)

247 Having established that the *mob4* mutant phenotype can be rescued by transgenic Mob4
248 expression, we next examined the temporal requirements for Mob4 function. We generated
249 a *ubi:loxP-Mob4EGFP-loxP-TagBFP* rescue transgenic line (Fig 6A) which exhibits robust
250 EGFP expression in various tissues (Fig 6- B:brain, B': endothelial cells, B'': muscles, B''':
251 epithelial cells). In epithelial cells, Mob4EGFP signal is clearly absent from cell membranes
252 (Fig 6B''', magenta asterisks), aligning with data from other studies. The Mob4 rescue
253 transgene was crossed into a *mob4* mutant background with a *hsp70l:Cre* transgene for heat-
254 shock-mediated deletion of Mob4 transgenic expression (Fig 6C). In the absence of heat
255 shock, the transgene was sufficient to rescue the *mob4* mutant phenotype in all cases (Fig 6
256 C'). Following heat shock at 30 hpf, mutant transgenic embryos exhibited typical *mob4*
257 mutant developmental phenotypes at 120 hpf, including pericardial and eye oedemas,
258 uninflated swim bladder, fin defects, and instances of haemorrhaging (Fig 6C''-C''''). Indeed,
259 no viable *hsp70l:Cre* heat-shocked *mob4* mutant transgenic adults were recovered following
260 early heat shock (Fig 6D), demonstrating that Cre-mediated deletion of the rescue construct
261 was robust. Having demonstrated a continuous (post-30 hpf) requirement for Mob4 function
262 in embryonic development, we next asked if Mob4 is required for adult physiology. Adult (6-
263 month-old) *mob4(-/-)*; *ubi:lox-Mob4EGFP-loxTagBFP (hemizygous); hsp70l:cre* fish were
264 subjected to heat shock and subsequently monitored (Fig 6D'). While the majority of *mob4*
265 mutant fish (9/13) died over a period of 5 months post-heat shock, limited mortality was
266 observed in a heterozygous *mob4* mutant transgenic control group (1/6). These results
267 indicate a continuous requirement for Mob4 function in embryonic development and adult
268 physiology.

269 We next examined the function of Mob4 in endothelial cells via the use of our conditional
270 rescue transgenic and a *kdrl:cre* EC-specific transgenic (Fig 6E). In *mob4(-/-); ubi:loxP-*
271 *Mob4EGFP-loxP-TAGBFP; kdrl:hRasmCherry* embryos without the *kdrl:cre* transgene (Fig
272 S2 A-A''), no signal was observed for Tag-BFP (Fig S2A). hRasmCherry labels all endothelial
273 cells (Fig S3A'). Mob4GFP was present in endothelial cells (yellow arrows S2A''). In *mob4(-*
274 */-); ubi:loxP-Mob4EGFP-loxP-TAGBFP; kdrl:hRasmCherry; kdrl:cre*, Cre was sufficient to
275 activate robust TagBFP in the vasculature (Fig S3B) with simultaneous reduction of GFP in
276 vascular cells (Fig S2B'-B'' orange asterisks). Interestingly, *mob4(-/-); ubi:loxP-Mob4EGFP-*
277 *loxP-TAGBFP; kdrl:Cre; kdrl:hRasmCherry* embryos appeared superficially normal at 120
278 hpf, with an absence of observable cranial hemorrhaging or cardiac oedemas (Fig 6F-F'')

279 and normal vascular patterning at 120 hpf (Fig 6G-G'''). Transgenic (GFP-positive) embryos
280 from these experiments were raised to adulthood and subsequently genotyped (Fig 6H). Of
281 the *mob4* mutants recovered (11/24 fish), three were additionally carriers of the *kdrl:Cre*
282 transgene, suggesting that Mob4 loss in endothelial cells alone may be insufficient for severe
283 or lethal phenotypes. Our results indicate that although global Mob4 loss leads to a spectrum
284 of defects in cardiovascular and neuronal development, Mob4 has pleiotropic tissue-specific
285 roles during development and adult life.

286 # Discussion

287 In this study, we have used the loss of Mob4 function in zebrafish as a proxy for examining
288 the role of the STRIPAK complex in vertebrate development, in particular vascular
289 development. Our proximal interactome of Mob4 in early zebrafish embryos confirms *in vitro*
290 work (Goudreault et al., 2009; Jeong et al., 2021; Kean et al., 2011) defining Mob4-STRIPAK
291 associations. As both Mob4 and Striatin3 loss led to similar defects in muscle and neuronal
292 development in zebrafish (Berger et al., 2022), these data argue that Mob4 is an integral
293 component of STRIPAK in zebrafish. We show that Mob4 loss leads to the eventual
294 cessation of blood flow in zebrafish, with defects in cardiac and vascular development.
295 Notably, *mob4* mutants demonstrate both intracranial haemorrhages at sites where
296 angiogenesis was at first apparently normal, and venous hypersprouting in the trunk
297 vasculature. Taken together, these results argue for Mob4/STRIPAK function regulating the
298 stability of developing vascular networks (at least in the case of the tail trunk vasculature) in
299 an endothelial cell-specific manner.
300 The signalling pathways that Mob4/STRIPAK act through and that are dysregulated in *mob4*
301 mutants remain to be determined. Components of the Wnt signalling pathway, including Axin
302 complex tumour suppressor adenomatous polyposis coli gene product APC (Apc), and
303 dishevelled segment polarity protein 3a (Dvl3a), are enriched in our Mob4 TurboID dataset.
304 Other enriched proteins relate to the neuronal phenotypes observed in *mob4* mutants,
305 including Filamin-interacting protein Filip1 and the atypical phosphatase Dusp27. Filip1
306 regulates dendritic spine development through modulation of non-muscle myosin 2b (Yagi et
307 al., 2014), while Dusp27 is required to establish proper Z-disc structure (Chen et al., 2023).
308 As Mob4 is also known to regulate cytoskeleton components in various systems, our data
309 raises the possibility that it acts through these and other regulators of cytoskeletal
310 development.
311
312 Although Mob4 has been shown to be enriched in various neuronal and glial tissues, current
313 data suggest that Mob4 has a broader role in organogenesis (Berger et al., 2022; Schulte et

al., 2010). Our mutant, rescue, and conditional loss-of-function models provide tools to understand the tissue-specific functions of Mob4. The rescue of trunk venous vasculature defects by *Lyve1:Mob4* strongly suggests an endothelial cell-specific function for Mob4. In contrast, *kdrl:Cre* (pan-EC)-mediated loss of Mob4 resulted in no discernible phenotypes. Unfortunately, the nature of the transgenic elements used for these experiments precluded being able to determine if Mob4 was completely lost in ECs, although we did observe (via expression of TAGBFP) robust recombination of the rescue transgene in ECs (Fig S3B). Given that incomplete Cre-mediated excision is observed for many zebrafish transgenic lines (Juan et al., 2024; Lalonde et al., 2022), and the possibility that multiple rescue transgene copies were present in transgenic lines used for these studies, it is possible that Mob4 was only lost in a mosaic manner in these experiments. It should be noted that *mob4* mutants, due to cardiac defects, lose blood flow over time, which in turn leads to well-characterized cardio-vascular defects (Kugler et al., 2021; Sehnert et al., 2002). The major vascular phenotypes observed in this study – cerebral haemorrhages and venous hypersprouting – have not been reported with reduced or absent blood flow in zebrafish. Interestingly, *mob4* mutant embryos exhibited haemorrhaging only in the head and not in the tail trunk vasculature, suggesting a specific function of Mob4 in maintaining the blood-brain barrier. Given the prominent neuronal defects observed in *mob4* mutants, and the role of secreted neuronal factors in cranial vasculature integrity (Hartmann et al., 2023), it is possible that Mob4 functions in multiple (EC, neuronal and perhaps other) cell types. More robust Cre deletor lines will be required to examine this, as the *hsp70l:Cre* transgenic appeared to be sufficient to greatly reduce Mob4 rescue expression.

Overall, we have shown that Mob4 functions as a component of the STRIPAK complex in zebrafish and has tissue-specific roles in the regulation of early cardiovascular and neuronal development. The latter, essential roles of Mob4 in adult physiology remain to be uncovered. However, the conditional rescue and loss of function tools we have developed, coupled with genetic and proteomic approaches, will, in the future, elucidate critical aspects of Mob4 and STRIPAK function.

# Materials and Methods

**Zebrafish and line maintenance**:

Adult AB/TL mixed strain zebrafish (Danio rerio) were maintained as per Canadian Council on Animal Care (CCAC) and The Hospital for Sick Children Animal Services (LAS) guidelines. The following previously described lines were used in our experiments: *Tg[kdrl:EGFP]* (*s843*); *Tg[gata1:dsred]* (*sd2*), *Tg[pdgfrb:Citrine]* (*s1010*), *Tg[tp1-*

348 *MmHbb:EGFP]* (*um14*), *Tg[kdrl:hRas-mCherry]* (*s896*), *Tg[hsp70l:Cre]* (*zdf13*),
349 *Tg[ngnl:Kate]* (*sk100*), *Tg[kdrl:Cre]* (*s898*).

350 **Generation of Crispr/Cas9 mutant line:**

351 The *mob4* (hsc205) mutant line was generated via use of CRISPR/Cas9 as described
352 previously (Jao et al., 2013). Cas9 was generated as previously described (Gagnon et al.,
353 2014). gRNA-Cas9 complex was injected High resolution melt (HRM) (Parant et al., 2009)
354 was used to test the efficacy of mutants with the following primers:
355 **F**:CGACGAAAGATCGTTATATGGTT, **R**:ATGAAGGACCCTTGTTGACATT Subsequent
356 genotyping for the *mob4* allele harbouring an 11bp deletion resolvable on an agarose gel
357 was carried out with PCR using the same primers.

358 **Plasmids and generation of transgenic lines**:

359 Gateway cloning was caried out with Gateway™ LR Clonase™ II Enzyme mix, and
360 Gateway™ BP Clonase™ II Enzyme mix from Thermos Fisher and various plasmids from
361 the Tol2kit (Kwan et al., 2007).

362 gRNA Plasmid: oligonucleotides TAGGAGATTATGGAGCCTCCAG and
363 AAACCTGGAGGCTCCATAATCT were annealed and cloned into pT7-gRNA with BsII.
364 gRNA was generated with BamHI/T7 MEGAshortscipt T7 (Invitrogen).

365 ***pCS2+Mob4***: The entire *mob4* CDS was amplified from 48 hpf *WT* cDNA with
366 **XhoI_mob4_F**: tatatCTCGAGatggtcatggc and **Mob4_XbaI_R**: tatataTCTAGAtcaggcatcgct
367 and cloned into pCS2+ with XhoI and XbaI.

368 ***pCS2+turboMob4EGFP****: mob4* was amplified *pCS2+Mob4* with **XhoI_mob4_F** and
369 **Mob4EGFP_OL_R**: TGCTCACCATGGCATCGCTT and *EGFP* was amplified with
370 **Mob4EGFP_OL_F**: AAGCGATGCCATGGTGAGCA and **XbaI_EGFP_R**:
371 TATATATCTAGATTACTTGTACAGCTCGT. Fusion PCR was carried out on the PCR
372 products with **XhoI_mob4_F** and **XbaI_EGFP_R**, to generate *mob4EGFP*, digested with
373 XhoI and XbaI and cloned into pCS2+ to generate *pCS2+mob4EGFP*. *Turbo* was amplified
374 with **XhoI_turbo_F**: tataCTCGAGGCAAACATGGCGAAAGATAAC and
375 **turbo_mob4_OL_R**: atgaccatAGATCCTCCCCC from PCS2+turbo (Rosenthal et al., 2021)
376 *mob4EGFP* was amplified with **turbo_mob4_OL_F**: GGGGGAGGATCTATGGTCAT and
377 **XbaI_Mob4_R**: tatataTCTAGAtcaggcatcgct from *pCS2+mob4EGFP*. *Turbomob4EGFP* was
378 amplified with fusion PCR with **XhoI_turbo_F** and **XbaI_Mob4_R** and cloned into pCS2+
379 with XhoI and XbaI. Capped *Turbomob4EGFP* mRNA was generated with SP6 mMessage
380 mMachine kit (ThermoFisher).

381 ***pME:TurboMob4EGFP***: *TurboMob4EGFP* was amplified from *pCS2+Turbomob4EGFP* with
382 **attb1_turbo_kozak_F**:ggggacaagtttgtacaaaaaagcaggctaagcaaacatggcgAAAGATAAC and
383 **attb2-EGFP-R**:ggggaccactttgtacaagaaagctgggtaTTACTTGTACAGCTCGTC and cloned
384 into pME with BP Clonase.

385 ***pDest[fli1a:mApple,cmlc2EGFP]***: Gateway cloning with plasmids from the. *p5E-fli1a*
386 (Lawson Lab), *pME:mApple* (Tol2kit) and *p3E:polyA* (Tol2kit) were gateway cloned with LR
387 Clonase (Gateway™ LR Clonase™ II Enzyme mix) into *pDestCG2* (Tol2kit) to generate
388 pDest*[fli1a:mApple,cmlc2EGFP]*.

389 ***pDest[lyve1:Mob4EGFP]***: p5E:Lyve1 (Tol2Kit), pME:Mob4EGFP, and p3E:polyA (Tol2kit)
390 were cloned into destination vector pDEst-CG2 (Tol2kit)

391 ***pDest[ubi:lox mSacrletNLS lox TurboMob4EGFP]***: the simpleswitch parent plasmid
392 *pDest[ubi:lox-mSacrletNLS-loxWasabi]* was from a previously published study (Burgess et
393 al., 2020). *TurboMob4EGFP* was amplified from *pCS2+TurboMob4EGFP* with
394 **Sbf1_Turbo_F**: tataCCTGCAGGcaaacatggcgAAAGATAACand and **AscI_EGFP-**
395 **STOP_rev**: tataggcgcgccTTACTTGTAC, digested with SbfI and AscI, and used to replace
396 wasabi in the simple switch plasmid to generate *pDest[ubi:lox-mSacrletNLS-*
397 *loxTurboMob4EGFP]*.

398 ***pDest[ubi: lox Mob4EGFP lox TagBFP]***. *Tag-BFP* was amplified with **Sbf1_Tag-BFP_F**:
399 tataCCTGCAGGcaaacatggtgagcgagc and **AscI_BFP_Rev**: tataGGCGCGCCttaattaagctt
400 and digested with SbfI and AscI and used to replace Wasabi in the Simpleswitch parent
401 plasmid to generate *pDest[ubi:lox-mSacrletNLS-loxTagBFP]*. Next M*ob4EGFP* was
402 amplified with **AgeI_Mob4_F:** tataaccggtgcaaacatggtcatggcggagg and **AgeI_EGFP_R**:
403 tataaccggtTTACTTGTACAGC and used to replace mScarletNLS between the lox sites in
404 *pDest[ubi:lox-mSacrletNLS-loxTagBFP]* to generate *pDest[ubi:lox-Mob4EGFP-loxTagBFP]*.

405 Transgenic lines were generated as described (Suster et al., 2011). Briefly 20-50 pg *pDest*
406 plasmid DNA and 100pg *tol2* mRNA was co-injected in single cell stage embryos. Embryos
407 with robust mosaic expression of selection markers were grown up and screened for F1
408 germline transmission to establish stable lines. The following hsc numbers are associated
409 with the lines generated in this work: *hsc201*:*Tg[fli1a:mApple,cmlc2:EGFP]*, *hsc202*:
410 *Tg[lyve1:Mob4:EGFP]*, *hsc203*: *Tg[ubi:lox mScarletNLS lox TurboMob4EGFP]*, *hsc204*:
411 *Tg[ubi: lox Mob4EGFP lox TagBFP]*. Plasmids for the generation of these lines or the lines
412 themselves are available upon request to ICS. The *Tg[mrc1a:EGFP] line* was generated from
413 a plasmid generously provided by the lab of Dr. Brant Weinstein and has been previously
414 described (Jung et al., 2017).

415 **Microscopy and image analysis**:

416 Whole embryo images were acquired using Zeiss AXIO Zoom V16. Confocal images were
417 acquired with Nikon A1R laser-scanning confocal microscope using either 20X or 40X water
418 immersion objectives. Images were analysed and processed with FijI (Schindelin et al.,
419 2012). Embryos were mounted in 0.8% low melt agarose in egg water in clear bottomed
420 round petri dishes, covered with embryo media, and placed on a heated plate holder at the
421 microscope for all live imaging. These embryos were carefully removed from agarose at the
422 end of imaging and genotyped as required.

423 **Proximity Dependant Biotinylation (BioID):**

424 BioID experiments followed the protocols as described in Rosenthal et al. 2021. To express
425 the TurboID fusion proteins 200pg of in vitro transcribed *TurboMob4EGFP* mRNA was
426 injected into single cell stage embryos. The embryos were incubated in egg water
427 supplemented with 800 µM biotin from 12 hpf. At 48 hpf labelling was terminated by transfer
428 to ice cold egg water. The embryos were then deyolked and frozen at -80°C. For protein
429 extraction and pulldown, the embryos lysis and streptavidin affinity purification were
430 performed as described. Proteins were prepared for mass spectrometry analysis as
431 described. Mass spectrometry acquisitions were performed using a ThemoFisher Fusion
432 Lumos mass spectrometer as described. Mass spectrometry data analysis was performed
433 as described. Briefly, ProteoWizard (Kessner et al., 2008) was used to convert the .RAW
434 files. The files were searched using Mascot (Perkins et al., 1999) and Comet (Eng et al.,
435 2013) against zebrafish sequences from the RefSeq database. The results from each search
436 engine were analysed with the Trans-Proteomic Pipeline (Deutsch et al., 2010) via the
437 iProphet pipeline (Shteynberg et al., 2011). Proteins with an iProphet probability ≥95% and
438 two unique peptides were used for analysis. For interaction scoring the SAINTexpress (Teo
439 et al., 2014) tool was used to score the probability of identified proteins being enriched above
440 background. Briefly, SAINTexpress uses the number of spectral counts for each prey
441 identified in the negative control runs compared against the average from the two replicates
442 of the experimental runs to calculate a Bayesian False Discovery Rate (BFDR); preys with a
443 BFDR ≤5% were considered high confidence. All data analysis was performed within the
444 ProHits laboratory information management system (LIMS) platform (Liu et al., 2010). For
445 data visualization, dot plots were generated using ProHits-viz (Knight et al., 2017) . To
446 perform Gene ontology gene set enrichment analysis human orthologs of the identified high
447 confidence proteins were retrieved using the DIOPT online tool (Hu et al., 2011). This
448 conversion was performed to take advantage of the much greater number of annotations
449 available for human genes than for the zebrafish. Gene ontology gene set enrichment

450 analysis was performed using the g:Profiler g:GOSt tool (Reimand et al., 2011) with default
451 settings.

452 # Acknowledgements

453 We wish to thank members of the Gingras and Scott labs for helpful discussions during the
454 execution of these experiments and writing of this manuscript. We would also like to thank
455 Dr. Brent Derry for valuable input during manuscript preparation and Dr. Brant Weinstein for
456 providing us with his *Tol2(mrc1a:EGFP)* construct. All zebrafish experiments were performed
457 in the zebrafish facility at The Hospital for Sick Children following the guidelines of the
458 institutional Animal Care Committee and the Canadian Council on Animal Care. We thank
459 Matthew Carpenter, Tyler Cunningham, Solange Prokop, Alejandro Salazar and their
460 associated work study students for expert care of animals used in this study. Proteomics
461 work was carried out at the Network Biology Collaborative Centre at the Lunenfeld-
462 Tanenbaum Research Institute by Brett Larsen and Cassandra Wong. SMR was supported
463 by Hospital for Sick Children Restracomp and Ontario Graduate Scholarship studentships.

464 This work was supported by funding from the Natural Sciences and Engineering Council of
465 Canada (NSERC, RGPIN-2017-06502 to ICS) and the Canadian Institutes of Health
466 Research (CIHR, PJT 153000 to ICS).

467 # References


468 Ando, K., Fukuhara, S., Izumi, N., Nakajima, H., Fukui, H., Kelsh, R.N., Mochizuki, N., 2016.
469 Clarification of mural cell coverage of vascular endothelial cells by live imaging of zebrafish.
470 Development (Cambridge) 143, 1328–1339. https://doi.org/10.1242/dev.132654

471 Baillat, G., Moqrich, A., Castets, F., Baude, A., Bailly, Y., Benmerah, A., Monneron, A., 2001.
472 Molecular Cloning and Characterization of Phocein, a Protein Found from the Golgi Complex
473 to Dendritic Spines, Molecular Biology of the Cell.

474 Bailly, Y.J.R., Castets, F., 2007. Phocein: A potential actor in vesicular trafficking at Purkinje cell
475 dendritic spines. Cerebellum 6, 344–352. https://doi.org/10.1080/14734220701225912

476 Bartoli, M., Monneron, A., Ladant, D., 1998. Interaction of calmodulin with striatin, a WD-repeat
477 protein present in neuronal dendritic spines. Journal of Biological Chemistry 273, 22248–
478 22253. https://doi.org/10.1074/jbc.273.35.22248

479 Berger, J., Berger, S., Currie, P.D., 2022. Mob4-dependent STRIPAK involves the chaperonin TRiC to
480 coordinate myofibril and microtubule network growth. PLoS Genet 18(6):e1010287.
481 https://doi.org/10.1371/journal.pgen.1010287

482 Bisoyi, P., Devi, P., Besra, K., Prasad, A., Jain, B.P., Goswami, S.K., 2022. The profile of expression of
483 the scaffold protein SG2NA(s) differs between cancer types and its interactome in normal vis-
484 a-vis breast tumor tissues suggests its wide roles in regulating multiple cellular pathways. Mol
485 Cell Biochem 477, 1653–1668. https://doi.org/10.1007/s11010-022-04401-8

486 Castets, F., Bartoli, M., Barnier, J., Baillat, G., Salin, P., Moqrich, A., Bourgeois, J.-P., Denizot, F.,
487 Rougon, G., Calothy, G., Monneron, A., 1996. A Novel Calmodulin-binding Protein, Belonging
488 to the WD-Repeat Family, Is Localized in Dendrites of a Subset of CNS Neurons. J Cell Biol 134,
489 1051–1062. https://doi.org/10.1083/jcb.134.4.1051

490 Chen, X., Li, Yanfeng, Xu, J., Cui, Y., Wu, Q., Yin, H., Li, Yuying, Gao, C., Jiang, L., Wang, H., Wen, Z.,
491 Yao, Z., Wu, Z., 2023. Styxl2 regulates de novo sarcomere assembly by binding to non-muscle
492 myosin IIs and promoting their degradation. Elife 12:RP87434.
493 https://doi.org/10.7554/eLife.87434

494 Couzens, A.L., Knight, J.D.R., Kean, M.J., Teo, G., Weiss, A., Dunham, W.H., Lin, Z.-Y., Bagshaw, R.D.,
495 Sicheri, F., Pawson, T., Wrana, J.L., Choi, H., Gingras, A.-C., 2013. Protein Interaction Network
496 of the Mammalian Hippo Pathway Reveals Mechanisms of Kinase-Phosphatase Interactions.
497 Syst Biol (Stevenage) 6(302):rs15. https://doi.org/10.1126/scisignal.2004712

498 Deutsch, E.W., Mendoza, L., Shteynberg, D., Farrah, T., Lam, H., Tasman, N., Sun, Z., Nilsson, E.,
499 Pratt, B., Prazen, B., Eng, J.K., Martin, D.B., Nesvizhskii, A.I., Aebersold, R., 2010. A guided tour
500 of the Trans-Proteomic Pipeline. Proteomics 10, 1150–1159.
501 https://doi.org/10.1002/pmic.200900375

502 Eng, J.K., Jahan, T.A., Hoopmann, M.R., 2013. Comet: An open-source MS/MS sequence database
503 search tool. Proteomics 13, 22–24. https://doi.org/10.1002/pmic.201200439

504 Gaengel, K., Genové, G., Armulik, A., Betsholtz, C., 2009. Endothelial-mural cell signaling in vascular
505 development and angiogenesis. Arterioscler Thromb Vasc Biol 29, 630–638.
506 https://doi.org/10.1161/ATVBAHA.107.161521

507 Goudreault, M., D'Ambrosio, L.M., Kean, M.J., Mullin, M.J., Larsen, B.G., Sanchez, A., Chaudhry, S.,
508 Chen, G.I., Sicheri, F., Nesvizhskii, A.I., Aebersold, R., Raught, B., Gingras, A.C., 2009. A PP2A
509 phosphatase high density interaction network identifies a novel striatin-interacting
510 phosphatase and kinase complex linked to the cerebral cavernous malformation 3 (CCM3)
511 protein. Molecular and Cellular Proteomics 8, 157–171.
512 https://doi.org/10.1074/mcp.M800266-MCP200

513 Haeberlé, A.M., Castets, F., Bombarde, G., Baillat, G., Bailly, Y., 2006. Immunogold localization of
514 phocein in dendritic spines. Journal of Comparative Neurology 495, 336–350.
515 https://doi.org/10.1002/cne.20895

516 Hu, Y., Flockhart, I., Vinayagam, A., Bergwitz, C., Berger, B., Perrimon, N., Mohr, S.E., 2011. An
517 integrative approach to ortholog prediction for disease-focused and other functional studies.
518 BMC Bioinformatics 12. https://doi.org/10.1186/1471-2105-12-357

519 Hwang, J., Pallas, D.C., 2014. STRIPAK complexes: Structure, biological function, and involvement in
520 human diseases. International Journal of Biochemistry and Cell Biology.
521 https://doi.org/10.1016/j.biocel.2013.11.021

522 Isogai, S., Lawson, N.D., Torrealday, S., Horiguchi, M., Weinstein, B.M., 2003. Angiogenic network
523 formation in the developing vertebrate trunk. Development 130, 5281–5290.
524 https://doi.org/10.1242/dev.00733

525 Jahan, M., Iwasa, H., Kuroyanagi, H., Hata, Y., 2021. Loss of Caenorhabditis elegans homologue of
526 human MOB4 compromises life span, health life span and thermotolerance. Genes to Cells 26,
527 798–806. https://doi.org/10.1111/gtc.12891

528 Jeong, B.C., Bae, S.J., Ni, L., Zhang, X., Bai, X. chen, Luo, X., 2021. Cryo-EM structure of the Hippo
529 signaling integrator human STRIPAK. Nat Struct Mol Biol 28, 290–299.
530 https://doi.org/10.1038/s41594-021-00564-y

531 Juan, T., Bellec, M., Cardoso, B., Athéa, H., Fukuda, N., Albu, M., Günther, S., Looso, M., Stainier,
532 D.Y.R., 2024. Control of cardiac contractions using Cre-lox and degron strategies in zebrafish.
533 Proc Natl Acad Sci U S A 121. https://doi.org/10.1073/pnas.2309842121

534 Jung, H.M., Castranova, D., Swift, M.R., Pham, V.N., Venero Galanternik, M., Isogai, S., Butler, M.G.,
535 Mulligan, T.S., Weinstein, B.M., 2017. Development of the larval lymphatic system in
536 zebrafish. Development (Cambridge) 144, 2070–2081. https://doi.org/10.1242/dev.145755

537 Kean, M.J., Ceccarelli, D.F., Goudreault, M., Sanches, M., Tate, S., Larsen, B., Gibson, L.C.D., Derry,
538 W.B., Scott, I.C., Pelletier, L., Baillie, G.S., Sicheri, F., Gingras, A.C., 2011. Structure-function
539 analysis of core STRIPAK proteins: A signaling complex implicated in Golgi polarization. Journal
540 of Biological Chemistry 286, 25065–25075. https://doi.org/10.1074/jbc.M110.214486

541 Kessner, D., Chambers, M., Burke, R., Agus, D., Mallick, P., 2008. ProteoWizard: Open source
542 software for rapid proteomics tools development. Bioinformatics 24, 2534–2536.
543 https://doi.org/10.1093/bioinformatics/btn323

544 Kim, J.W., Berrios, C., Kim, M., Schade, A.E., Adelmant, G., Yeerna, H., Damato, E., Iniguez, A.B.,
545 Florens, L., Washburn, M.P., Stegmaier, K., Gray, N.S., Tamayo, P., Gjoerup, O., Marto, J.A.,
546 Decaprio, J., Hahn, W.C., 2020. STRIPAK directs PP2A activity toward MAP4K4 to promote
547 oncogenic transformation of human cells. Elife 9. https://doi.org/10.7554/eLife.53003

548 Kinney, B.A., Al Anber, A., Row, R.H., Tseng, Y.J., Weidmann, M.D., Knaut, H., Martin, B.L., 2020.
549 Sox2 and Canonical Wnt Signaling Interact to Activate a Developmental Checkpoint
550 Coordinating Morphogenesis with Mesoderm Fate Acquisition. Cell Rep 33.
551 https://doi.org/10.1016/j.celrep.2020.108311

552 Knight, J.D.R., Choi, H., Gupta, G.D., Pelletier, L., Raught, B., Nesvizhskii, A.I., Gingras, A.C., 2017.
553 ProHits-viz: A suite of web tools for visualizing interaction proteomics data. Nat Methods.
554 https://doi.org/10.1038/nmeth.4330

555 Kück, U., Beier, A.M., Teichert, I., 2016. The composition and function of the striatin-interacting
556 phosphatases and kinases (STRIPAK) complex in fungi. Fungal Genetics and Biology 90, 31–38.
557 https://doi.org/10.1016/j.fgb.2015.10.001

558 Kugler, E., Snodgrass, R., Bowley, G., Plant, K., Serbanovic-Canic, J., Hamilton, N., Evans, P.C., Chico,
559 T., Armitage, P., 2021. The effect of absent blood flow on the zebrafish cerebral and trunk
560 vasculature. Vascular Biology 3, 1–16. https://doi.org/10.1530/vb-21-0009

561 Kwan, K.M., Fujimoto, E., Grabher, C., Mangum, B.D., Hardy, M.E., Campbell, D.S., Parant, J.M.,
562 Yost, H.J., Kanki, J.P., Chien, C. Bin, 2007. The Tol2kit: A multisite gateway-based construction
563 Kit for Tol2 transposon transgenesis constructs. Developmental Dynamics 236, 3088–3099.
564 https://doi.org/10.1002/dvdy.21343

565 Lahav-Ariel, L., Caspi, M., Nadar-Ponniah, P.T., Zelikson, N., Hofmann, I., Hanson, K.K., Franke,
566 W.W., Sklan, E.H., Avraham, K.B., Rosin-Arbesfeld, R., 2019. Striatin is a novel modulator of
567 cell adhesion. FASEB Journal 33, 4729–4740. https://doi.org/10.1096/fj.201801882R

568 Lalonde, R.L., Kemmler, C.L., Riemslagh, F.W., Aman, A.J., Kresoja-Rakic, J., Moran, H.R.,
569 Nieuwenhuize, S., Parichy, D.M., Burger, A., Mosimann, C., 2022. Heterogeneity and genomic
570 loci of ubiquitous transgenic Cre reporter lines in zebrafish. Developmental Dynamics 251,
571 1754–1773. https://doi.org/10.1002/dvdy.499

572 Lant, B., Yu, B., Goudreault, M., Holmyard, D., Knight, J.D.R., Xu, P., Zhao, L., Chin, K., Wallace, E.,
573 Zhen, M., Gingras, A.C., Derry, W.B., 2015. CCM-3/STRIPAK promotes seamless tube extension
574 through endocytic recycling. Nat Commun 6. https://doi.org/10.1038/ncomms7449

575 Li, D., Musante, V., Zhou, W., Picciotto, M.R., Nairn, A.C., 2018. Striatin-1 is a B subunit of protein
576 phosphatase PP2A that regulates dendritic arborization and spine development in striatal
577 neurons. Journal of Biological Chemistry 293, 11179–11194.
578 https://doi.org/10.1074/jbc.RA117.001519

579 Liu, G., Zhang, J., Larsen, B., Stark, C., Breitkreutz, A., Lin, Z.Y., Breitkreutz, B.J., Ding, Y., Colwill, K.,
580 Pasculescu, A., Pawson, T., Wrana, J.L., Nesvizhskii, A.I., Raught, B., Tyers, M., Gingras, A.C.,
581 2010. ProHits: Integrated software for mass spectrometry-based interaction proteomics. Nat
582 Biotechnol. https://doi.org/10.1038/nbt1010-1015

583 Madsen, C.D., Hooper, S., Tozluoglu, M., Bruckbauer, A., Fletcher, G., Erler, J.T., Bates, P.A.,
584 Thompson, B., Sahai, E., 2015. STRIPAK components determine mode of cancer cell migration
585 and metastasis. Nat Cell Biol 17, 68–80. https://doi.org/10.1038/ncb3083

586 Moreno, C.S., Park, S., Nelson, K., Ashby, D., Hubalek, F., Lane, W.S., Pallas, D.C., 2000. WD40
587 Repeat Proteins Striatin and S/G 2 Nuclear Autoantigen Are Members of a Novel Family of

588 Calmodulin-binding Proteins That Associate with Protein Phosphatase 2A. Journal of Biological
589 Chemistry 275, 5257–5263. https://doi.org/10.1074/jbc.275.8.5257

590 Myers, P.Z., 1985. Spinal Motoneurons of the Larval Zebrafish. J Comp Neurol 236, 232555–561.
591 https://doi.org/10.1002/cne.902360411

592 Myers, P.Z., Eisen, J.S., Westerfield, M., 1986. Development and Axonal Outgrowth of Identified
593 Motoneurons in the Zebrafish. The Journal of Neuroscience 6, 2278–2289.
594 https://doi.org/10.1523/JNEUROSCI.06-08-02278.1986

595 Nadar-Ponniah, P.T., Taiber, S., Caspi, M., Koffler-Brill, T., Dror, A.A., Siman-Tov, R., Rubinstein, M.,
596 Padmanabhan, K., Luxenburg, C., Lang, R.A., Avraham, K.B., Rosin-Arbesfeld, R., 2020. Striatin
597 Is Required for Hearing and Affects Inner Hair Cells and Ribbon Synapses. Front Cell Dev Biol 8.
598 https://doi.org/10.3389/fcell.2020.00615

599 Perkins, D.N., Pappin, D.J.C., Creasy, D.M., Cottrell, J.S., 1999. Probability-based protein
600 identification by searching sequence databases using mass spectrometry data, in:
601 Electrophoresis. Wiley-VCH Verlag, pp. 3551–3567. https://doi.org/10.1002/(SICI)1522-
602 2683(19991201)20:18<3551::AID-ELPS3551>3.0.CO;2-2

603 Qiu, L.M., Sun, Y.H., Chen, T.T., Chen, J.J., Ma, H.T., 2020. STRIP2, a member of the striatin-
604 interacting phosphatase and kinase complex, is implicated in lung adenocarcinoma cell
605 growth and migration. FEBS Open Bio 10, 351–361. https://doi.org/10.1002/2211-5463.12785

606 Quillien, A., Moore, J.C., Shin, M., Siekmann, A.F., Smith, T., Pan, L., Moens, C.B., Parsons, M.J.,
607 Lawson, N.D., 2014. Distinct Notch signaling outputs pattern the developing arterial system.
608 Development (Cambridge) 141, 1544–1552. https://doi.org/10.1242/dev.099986

609 Rajan, A.M., Ma, R.C., Kocha, K.M., Zhang, D.J., Huang, P., 2020. Dual function of perivascular
610 fibroblasts in vascular stabilization in zebrafish. PLoS Genet 16.
611 https://doi.org/10.1371/journal.pgen.1008800

612 Reimand, J., Arak, T., Vilo, J., 2011. G:Profiler - A web server for functional interpretation of gene
613 lists (2011 update). Nucleic Acids Res 39. https://doi.org/10.1093/nar/gkr378

614 Ribeiro, P.S., Josué, F., Wepf, A., Wehr, M.C., Rinner, O., Kelly, G., Tapon, N., Gstaiger, M., 2010.
615 Combined Functional Genomic and Proteomic Approaches Identify a PP2A Complex as a
616 Negative Regulator of Hippo Signaling. Mol Cell 39, 521–534.
617 https://doi.org/10.1016/j.molcel.2010.08.002

618 Rosenthal, S.M., Misra, T., Abdouni, H., Branon, T.C., Ting, A.Y., Scott, I.C., Gingras, A.C., 2021. A
619 toolbox for efficient proximity-dependent biotinylation in Zebrafish embryos. Molecular and
620 Cellular Proteomics 20. https://doi.org/10.1016/j.mcpro.2021.100128

621 Santos, I.B., Wainman, A., Garrido-Maraver, J., Pires, V., Riparbelli, M.G., Kovács, L., Callaini, G.,
622 Glover, D.M., Tavares, Á.A., 2023. Mob4 is essential for spermatogenesis in Drosophila
623 melanogaster. Genetics 224. https://doi.org/10.1093/genetics/iyad104

624 Schad, E.G., Petersen, C.P., 2020. STRIPAK Limits Stem Cell Differentiation of a WNT Signaling
625 Center to Control Planarian Axis Scaling. Current Biology 30, 254-263.e2.
626 https://doi.org/10.1016/j.cub.2019.11.068

627 Schindelin, J., Arganda-Carreras, I., Frise, E., Kaynig, V., Longair, M., Pietzsch, T., Preibisch, S.,
628 Rueden, C., Saalfeld, S., Schmid, B., Tinevez, J.Y., White, D.J., Hartenstein, V., Eliceiri, K.,
629 Tomancak, P., Cardona, A., 2012. Fiji: An open-source platform for biological-image analysis.
630 Nat Methods. https://doi.org/10.1038/nmeth.2019

631 Schulte, J., Sepp, K.J., Jorquera, R.A., Wu, C., Song, Y., Hong, P., Troy Littleton, J., 2010.
632 DMob4/Phocein regulates synapse formation, axonal transport, and microtubule
633 organization. Journal of Neuroscience 30, 5189–5203.
634 https://doi.org/10.1523/JNEUROSCI.5823-09.2010

635 Sehnert, A.J., Huq, A., Weinstein, B.M., Walker, C., Fishman, M., Stainier, D.Y.R., 2002. Cardiac
636 troponin T is essential in sarcomere assembly and cardiac contractility. Nat Genet 31, 106–
637 110. https://doi.org/10.1038/ng875

638 Sepp, K.J., Hong, P., Lizarraga, S.B., Liu, J.S., Mejia, L.A., Walsh, C.A., Perrimon, N., 2008.
639 Identification of neural outgrowth genes using genome-wide RNAi. PLoS Genet 4.
640 https://doi.org/10.1371/journal.pgen.1000111

641 Shi, Z., Jiao, S., Zhou, Z., 2016. STRIPAK complexes in cell signaling and cancer. Oncogene.
642 https://doi.org/10.1038/onc.2016.9

643 Shteynberg, D., Deutsch, E.W., Lam, H., Eng, J.K., Sun, Z., Tasman, N., Mendoza, L., Moritz, R.L.,
644 Aebersold, R., Nesvizhskii, A.I., 2011. iProphet: Multi-level integrative analysis of shotgun
645 proteomic data improves peptide and protein identification rates and error estimates.
646 Molecular and Cellular Proteomics 10. https://doi.org/10.1074/mcp.M111.007690

647 Suster, M.L., Abe, G., Schouw, A., Kawakami, K., 2011. Transposon-mediated BAC transgenesis in
648 zebrafish. Nature Protocols 2011 6:12 6, 1998–2021. https://doi.org/10.1038/nprot.2011.416

649 Tang, Y., Fang, G., Guo, F., Zhang, H., Chen, X., An, L., Chen, M., Zhou, Li, Wang, W., Ye, T., Zhou, Lei,
650 Nie, P., Yu, H., Lin, M., Zhao, Y., Lin, X., Yuan, Z., Jiao, S., Zhou, Z., 2020. Selective Inhibition of
651 STRN3-Containing PP2A Phosphatase Restores Hippo Tumor-Suppressor Activity in Gastric
652 Cancer. Cancer Cell 38, 115-128.e9. https://doi.org/10.1016/j.ccell.2020.05.019

653 Teo, G., Liu, G., Zhang, J., Nesvizhskii, A.I., Gingras, A.C., Choi, H., 2014. SAINTexpress:
654 Improvements and additional features in Significance Analysis of INTeractome software. J
655 Proteomics 100, 37–43. https://doi.org/10.1016/j.jprot.2013.10.023

656 Trammell, M.A., Mahoney, N.M., Agard, D.A., Vale, R.D., 2008. Mob4 plays a role in spindle
657 focusing in Drosophila S2 cells. J Cell Sci 121, 1284–1292. https://doi.org/10.1242/jcs.017210

658 Vanhollebeke, B., Stone, O.A., Bostaille, N., Cho, C., Zhou, Y., Maquet, E., Gauquier, A., Cabochette,
659 P., Fukuhara, S., Mochizuki, N., Nathans, J., Stainier, D.Y., 2015. Tip cell-specific requirement
660 for an atypical Gpr124- and Reck-dependent Wnt/β-catenin pathway during brain
661 angiogenesisAbstract. Elife. https://doi.org/10.7554/eLife.06489.001

662 Yagi, H., Nagano, T., Xie, M.J., Ikeda, H., Kuroda, K., Komada, M., Iguchi, T., Tariqur, R.T., Morikubo,
663 S., Noguchi, K., Murase, K., Okabe, M., Sato, M., 2014. Filamin A-interacting protein (FILIP) is a
664 region-specific modulator of myosin 2b and controls spine morphology and NMDA receptor
665 accumulation. Sci Rep 3. https://doi.org/10.1038/srep06353

666

# Figure Legends

**Figure 1**: ***In vivo* interactome of Mob4 in zebrafish embryos** (A) Schematic of pipeline to conduct BioID *in vivo*. *In vitro* transcribed *TurboMob4EGFP* mRNA is injected at the single cell stage. Embryos are transferred to 800µM biotin containing egg water at 16 hpf and collected for protein purification at 48 hpf. Biotinylated proteins are enriched on streptavidin beads and further analysed with mass spectrometry. (B) Proteins with a BFDR ≤5% after SAINT analysis are shown. The average abundance (by spectral count) is visualized by the colour of the dot on the dot plot. (C) Gene Ontology (GO) term enrichment analysis results for the Human orthologues of the high confidence (BFDR ≤5%) hits.

**Figure 2**: **Crispr/Cas9 mediated Mob4 lof leads to cardiovascular defects** (A) Schematic of *mob4* locus with gRNA targeting site (top panel) and corresponding WT protein and mutant peptide expected (bottom panel). Red rectangle in *mob4* mutant peptide represents non conserved residues induced by the mutation before eventual STOP codon. (B) Sequence traces of 11bp deletion in *mob4* mutant allele (top panel) compared to *WT* sequence (bottom panel). (C-C') Brightfield images of *control* (C) and *mob4 mutant* (C', black arrowhead: cardiac oedema) embryos at 56 hpf. (D-D'') *gata1:dsred* labelled blood cells in *control* (D) and *mob4* mutant (D', yellow arrowhead: haemorrhage, white arrowhead: loss of blood flow). (E-E'''') Representative brightfield images of degrees of cranial haemorrhaging (blue arrowheads) and cardiac oedemas (magenta asterisks) at 72 hpf (E'-cardiac oedema no visible haemorrhage, E''-cardiac oedema + cranial haemorrhage E''- mild cardiac oedema + two fore- and hindbrain haemorrhages, E'''- slight cardiac oedema + large hindbrain haemorrhage). (F-H''') heart morphology in 72 hpf *control* (F-F'') and *mob4 mutant* (G-G'', H-H'') embryos. A: Atrium. V: Ventricle. Orange asterisks: oedema pericardial space. White arrowheads: AVC, Atrioventricular canal. I''', J''', K''': single slices of z-stacks showing endocardium (*kdrl:hRasmCherry*) and myocardium (*myl7:EGFP*). Scale bar = 100um.

**Figure 3**: **Mob4 lof leads to cranial haemorrhages and vascular defects:** (A-D'') Cranial vasculature (*kdrl:EGFP*) and blood cells (*gata1:dsRed*) in *control* (A-A'': 48 hpf, C-C'': 96 hpf) and *mob4 mutant* embryos (B-B'': 48hpf, D-D'' 96hpf); Yellow arrowhead: haemorrhage, white asterisks: collapsed blood vessels). (E-F'') Snapshots of time lapse videos of cranial vascular development and blood flow from 36 hpf in *WT*(E-E'') and *mob4 mutant* (F-F''). Yellow asterisks: Haemorrhages. (G-I'') Snapshots of time lapse videos of tail trunk vasculature development and blood flow from 36 hpf in *WT*(G-G'') and *mob4 mutant* (H-H'', I-I'') embryos. Over sprouting endothelial cells are indicated with asterisks across time; each colour follows a single vessel. DMJ: dorsal midline junction, MsV: Mesencephalic Vein, ISV: intersegmental vessels, DA: dorsal aorta, CV: caudal vein, CVP: caudal venous plexus.

**Figure 4**: **Mob4 lof leads to defects in sprouting of lymphatic derived vessels** (A-C'') Tail trunk vasculature (*kdrl:hRasmCherry*) and notch signalling reporter (*tp1:GFP*) in *control* (A-A'') and *mob4 mutant* (B-B'', C-C'') in 80 hpf embryos. mCherry positive and GFP negative hypersprouting ECs are marked with yellow asterisks. Cyan asterisk: DA, orange asterisk: notochord. (D-E'') Tail trunk vasculature in double transgenic (*kdrl:hRasmCherry;mrc1:EGFP*) to label all ECs with mCherry and lymphatic ECs are cells

712 in *control* (D-D'') and *mob4 mutant* (E-E'', C-C'') in 72 hpf embryos. Cherry and GFP double
713 positive hypersprouting ECs are marked with asterisks. (F) Schematic for transgenic to
714 express Mob4EGFP in lymphatic cells. (G'-J''')_*wt* (G-G'') *mob4*
715 *mutant;kdrl:hRasmCherry;(lyve1:Mob4EGFP;cmlc2:EGFP)* and Mob4 loss (I-J'') *mob4*
716 *mutant;kdrl:hRasmCherry;* (*lyve1:Mob4EGFP;cmlc2:EGFP)* embryos at 3.5dpf. Scale bar-
717 100µm. CVP: Caudal Venous Plexus, DA: Dorsal Aorta

718 **Figure 5**: **Mob4 lof leads to neuronal defects** (A-A'') Cranial neurons in *control* (A) and
719 *mob4 mutant* (A'-A'') 84 hpf embryos. Neuronal bundles are marked with asterisks (WT:
720 green asterisks, aberrant: magenta asterisks). (B-B'') tail trunk motor neurons in *control* (B)
721 and *mob4 mutant* (B'-B''m blue asterisks motor neurons with no outgrowth, magenta
722 asterisks MN with hypersprouting) 84 hpf embryos. (A-B''') Snapshots of time lapse imaging
723 of development of motor neurons (*ngnl:mKate*) in tail trunk of *control* (C-C''') and *mob4*
724 *mutant* (D-D''') embryos. Time stamps (hh:mm) represent time after start of imaging (00:00).
725 Asterisk colours follow single motor neurons. Selected aberrant (D'-*, D''-*) neurons are
726 magnified to enhance detail. Scale bar=100µm.

727

728 **Figure 6**: **Mob4 has cell specific roles during development** (A) Schematic of rescue
729 transgene. (B-B'') Localisation of Mob4EGFP in the brain (B), endothelial cells (B', yellow
730 asterisk), notochord (B' orange asterisk), epithelial cells (B''', magenta asterisk exclusion of
731 Mob4EGFP from cell membrane). (C) Schematic for heat shock induced recombination of
732 *Mob4EGFP* from rescue transgene. (C-C''') Heat shocked *mob4*$^{(-/-)}$ embryos with rescue
733 transgene, *ubi:loxMob4EGFPloxTAGBFP* (C') without *hsp70l:Cre* (C''-C''') with *hsp70l:Cre*.
734 (D) Top panel: schematic of experiment to determine long term efficiency of heat shock
735 induced Mob4 loss model. bottom panel: genotypes of resultant adults. (D') Top panel:
736 schematic of experiment to determine heat shock induced Mob4 loss in adults, bottom panel:
737 score of lethality in *mob4 mutant* vs *control* adults with rescue transgene
738 *ubi:loxMob4EGFPloxTAGBFP*. All adult fish are positive for *hsp70l:Cre*. (E) Schematic for
739 Vascular Mob4 loss model. *kdrl:Cre* induced recombination of *Mob4EGFP* from rescue
740 transgene *ubi:loxMob4EGFPloxTAGBFP* in endothelial cells. (F-F'') early development in
741 endothelial Mob4 loss model. Representative brightfield images of whole embryos at 5 dpf.
742 (F) *mob4*$^{(+/-)}$;*ubi:loxMob4EGFPloxTAGBFP;kdrl:Cre*, *control* (F') *mob4(-/-*
743 *)*;*ubi:loxMob4EGFPloxTAGBFP*;*kdrl:Cre*, vascular Mob4 loss (F'') *mob4 mutant* embryo,
744 global mob4 loss. (G-G''') vascular development in vascular Mob4 loss model with
745 *kdrl:hRasmCherry* labelled vasculature at 5dpf. (G, G') brain and tail trunk vasculature in
746 *mob4(-/-)*;*ubi:loxMob4EGFPloxTAGBFP* (control, rescued embryos). (G''-G''') brain and tail
747 trunk vasculature in *mob4(-/-)*;*ubi:loxMob4EGFPloxTAGBFP;kdrl:Cre* (vascular Mob4 loss).
748 (H) Left panel: Schematic to determine effect of vascular Mob4 loss in adults. Right panel:
749 genotyping of adults. Scale bar=100µm.

750

751 **Figure S1**: **Pericyte localisation in vasculature of *mob4 mutant* embryos**. *pdgfrb:Citrine*
752 labels pericytes with Citrine and *kdrl:hRasmCherry* labels all ECs. (A-C'') Projections of
753 confocal z-stacks of head (A-C'') and tail trunk (D-F'') of 80 hpf embryos imaged laterally. (A-
754 A'', D-D'') *control* (B-C'', E-F'') two representative *mob4 mutant* embryos each for head and
755 tail trunk vasculature. Pericytes associated with ECs are indicated with yellow arrowheads.
756 Scale bar=100µm

757

**Figure S2: Action of Switch Transgene in the vasculature.** (A-B'') Confocal images of vasculature in the tail trunk. (A-A'') *mob4(-/-);ubi:loxMob4EGFPlox TagBFP* (B-B'') *mob4(-/-);ubi:loxMob4EGFPlox TagBFP; kdrl:Cre.* Scale bar=100µm

**Figure S3:** (A) Schematic for rescue transgene (B) Schematic of heat shock dependent rescue experiment. Heat shock carried out at 20 hpf and 30 hpf. Whole embryos imaged at 5dpf. All embryos C-F' are positive for *ubi:loxP-mScarletNLS-LoxP-TurboMob4EGFP* (C) only ubi:loxP-mScarletNLS-loxP-TurboMob4EGFP (D) ubi:loxP-mScarletNLS-loxP-*TurboMob4EGFP;hsp70l:Cre* (E-E') *mob4(-/-);ubi:loxP-mScarletNLS-loxP-TurboMob4EGFP* (F-F') *mob4(-/-);ubi:loxP-mScarletNLS-loxP-TurboMob4EGFP;hsp70l:Cre* rescued embryos

**Supplementary Movie1**: Time lapse imaging of lateral head vasculature starting at 54 hpf in *kdrl:EGFP*;*gata1:dsRed* double transgenic embryos. EGFP labels all ECs and dsREd (A) *control* (B-D) *mob4 mutant* embryos. GFF. Asterisks show instances of haemorrhage in B and D and vascular anomalies in (C). Scale bar=100µm.

**Supplementary Movie 2**: Time lapse imaging of lateral tail trunk vasculature starting around 54 hpf in *kdrl:EGFP*;*gata1:dsRed* double transgenic embryos (A) *control* (B-D) *mob4 mutant* embryos. Asterisks show aberrantly sprouting ECs. Scale bar=100µm.

**Supplementary Movie 3**: Time lapse imaging of lateral tail trunk vasculature starting around 56 hpf in *tp1:EGFP*; *kdrl:hRAsmCherry* double transgenic embryos. (A-A'') *control* (B-B'', C-C'') *mob4 mutant* embryos. Asterisks label hypersprouting ECs positive for mCherry and negative for EGFP in *mob4 mutant* embryos

**Supplementary Movie 4**: Time lapse imaging of motor neurons in the lateral tail trunk starting around 54 hpf in *ngn1:mKate* transgenic embryos. (A) *control* (B) *mob4 mutant*. Asterisks marks irregularities in neuron outgrowth. Scale bar=100µm.

787 # Figures

**Figure 1**

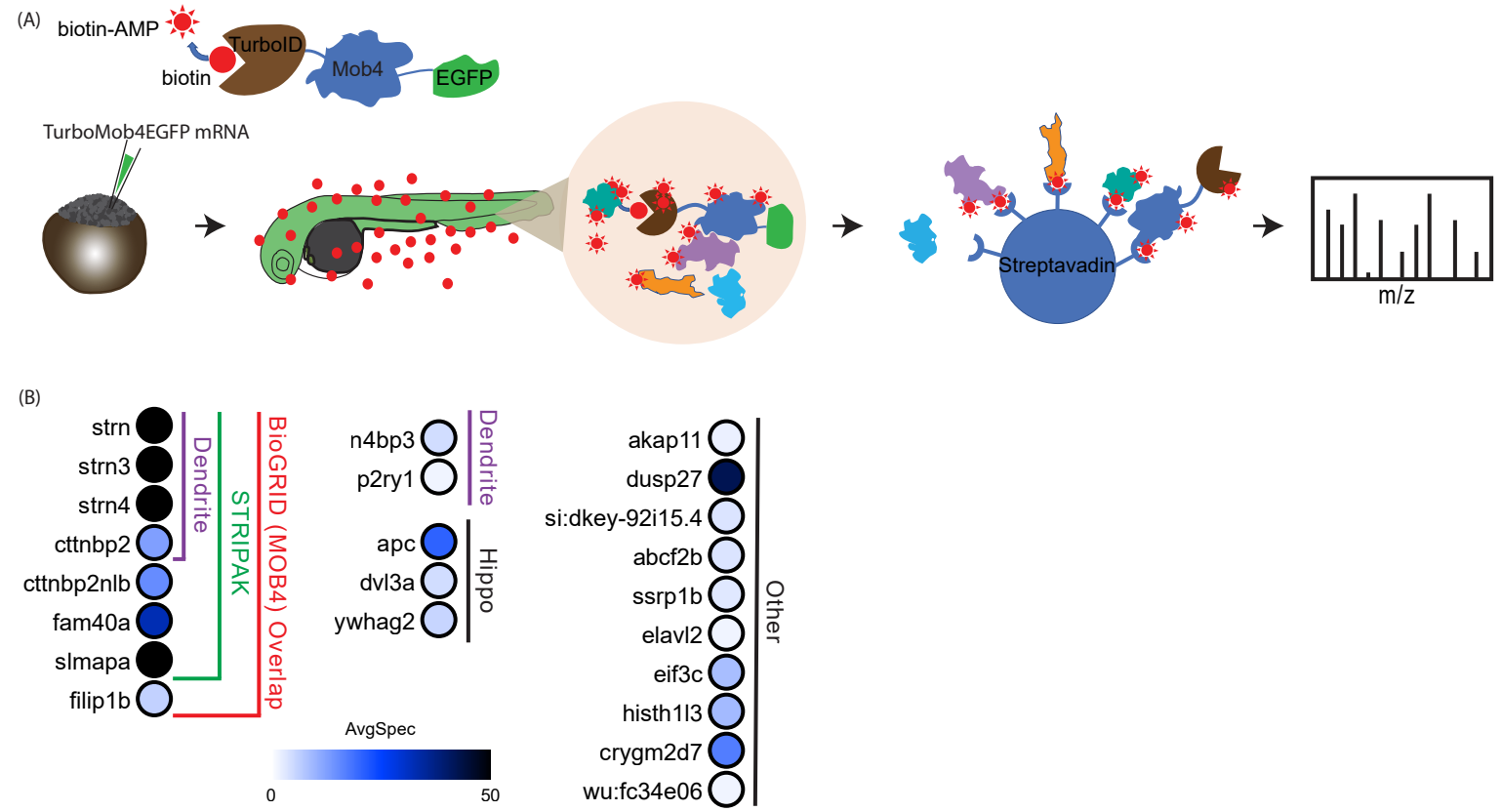


(C)

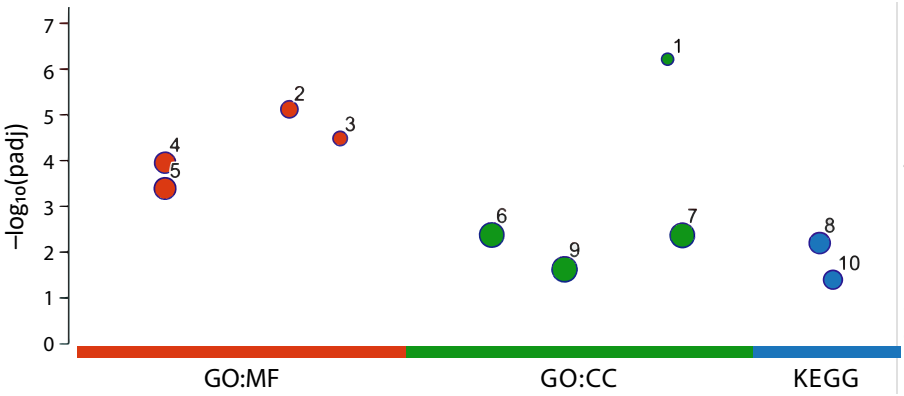


| | term_name | adjusted_p_value |
|---|---|---|
| 1 | FAR/SIN/STRIPAK complex | 6.32E-07 |
| 2 | protein phosphatase 2A binding | 7.84899E-06 |
| 3 | armadillo repeat domain binding | 3.39881E-05 |
| 4 | protein phosphatase binding | 0.00011511 |
| 5 | phosphatase binding | 0.000421358 |
| 6 | dendrite | 0.004371587 |
| 7 | dendritic tree | 0.004452632 |
| 8 | Hippo signaling pathway | 0.006540971 |
| 9 | somatodendritic compartment | 0.024581578 |
| 10 | Basal cell carcinoma | 0.041389733 |

Figure 2

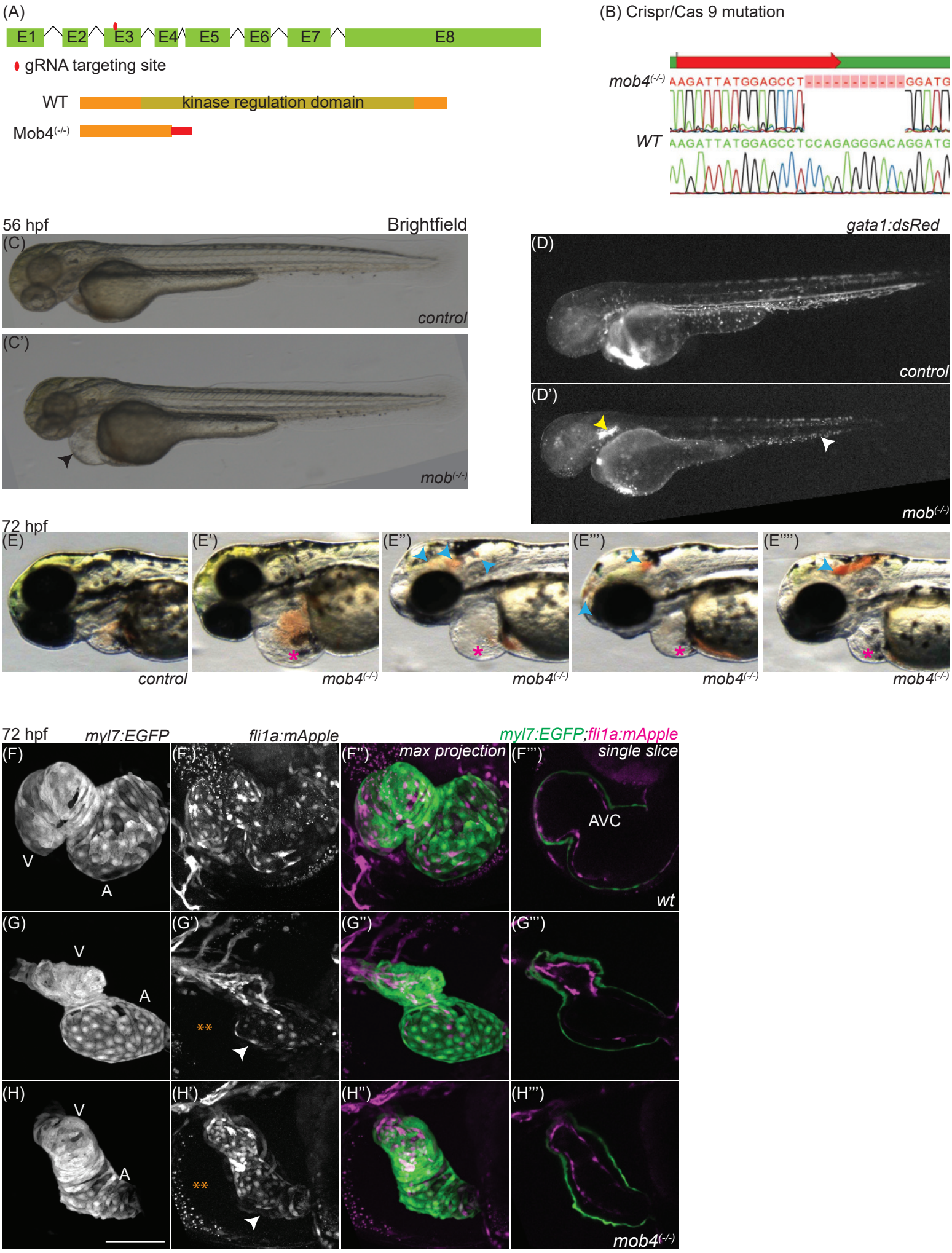
(A)
E1
E2
E3
E4
E5
E6
E7
E8
gRNA targeting site
WT
kinase regulation domain
Mob4(-/-)
(B) Crispr/Cas 9 mutation
mob4(-/-)
AAGATTATGGAGCCT----------GGATG
WT
AAGATTATGGAGCCTCCAGAGGGACAGGATG
56 hpf
Brightfield
(C)
control
(C')
mob(-/-)
gata1:dsRed
(D)
control
(D')
mob(-/-)
72 hpf
(E)
control
(E')
mob4(-/-)
(E'')
mob4(-/-)
(E''')
mob4(-/-)
(E'''')
mob4(-/-)
72 hpf
myl7:EGFP
fli1a:mApple
myl7:EGFP;fli1a:mApple
(F)
V
A
(F')
(F'')
max projection
(F''')
single slice
AVC
wt
(G)
V
A
(G')
**
(G'')
(G''')
(H)
V
A
(H')
**
(H'')
(H''')
mob4(-/-)

**Figure 3**

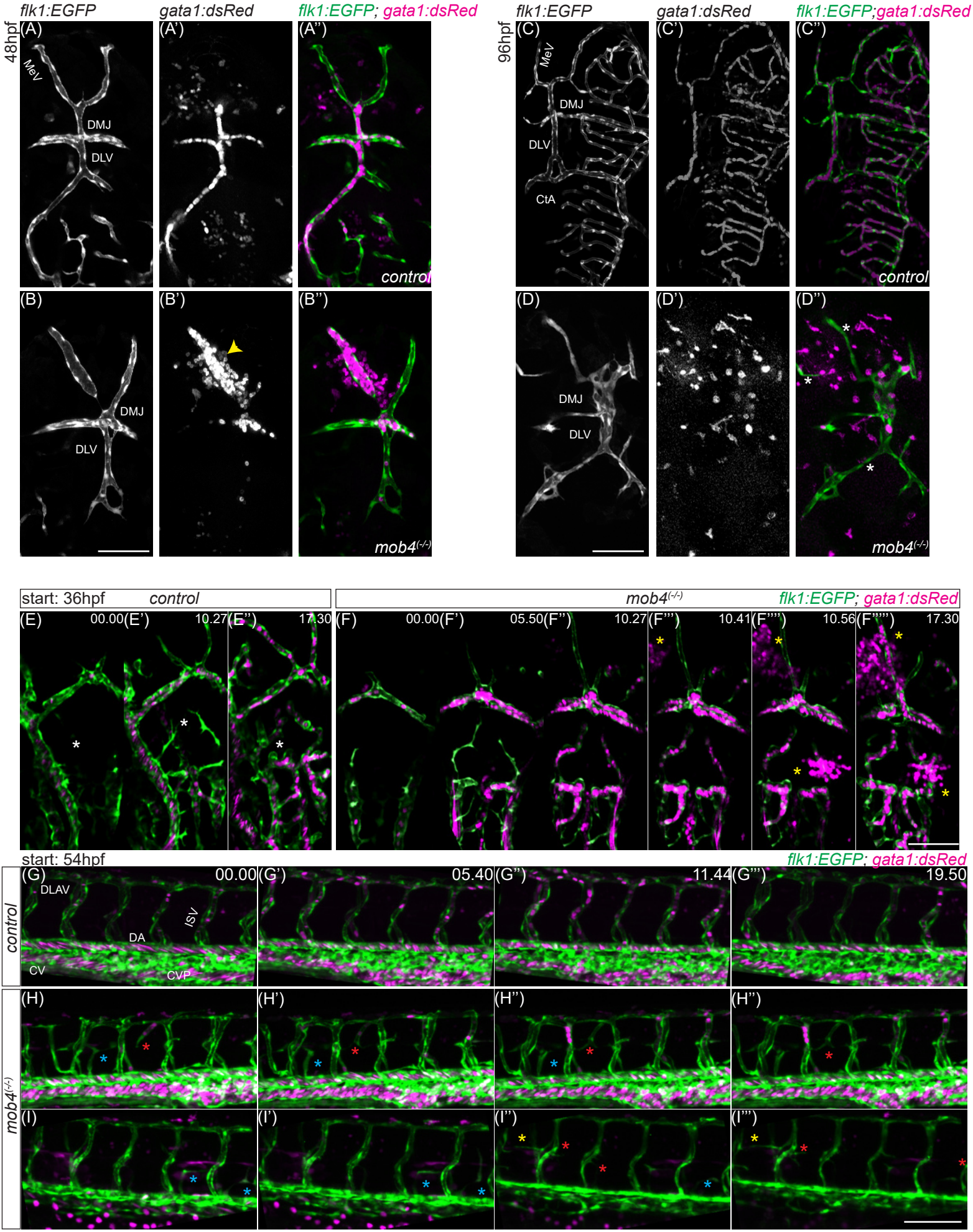
flk1:EGFP
gata1:dsRed
flk1:EGFP; gata1:dsRed
48hpf
(A)
(A')
(A")
MeV
DMJ
DLV
control
(B)
(B')
(B")
DMJ
DLV
mob4(-/-)
96hpf
(C)
(C')
(C")
MeV
DMJ
DLV
CtA
control
(D)
(D')
(D")
DMJ
DLV
mob4(-/-)
start: 36hpf
control
mob4(-/-)
(E)
00.00
(E')
10.27
(E")
17.30
(F)
00.00
(F')
05.50
(F")
10.27
(F''')
10.41
(F'''')
10.56
(F''''')
17.30
start: 54hpf
(G)
00.00
(G')
05.40
(G")
11.44
(G''')
19.50
DLAV
ISV
DA
CV
CVP
(H)
(H')
(H")
(H")
(I)
(I')
(I")
(I''')

**Figure 4**

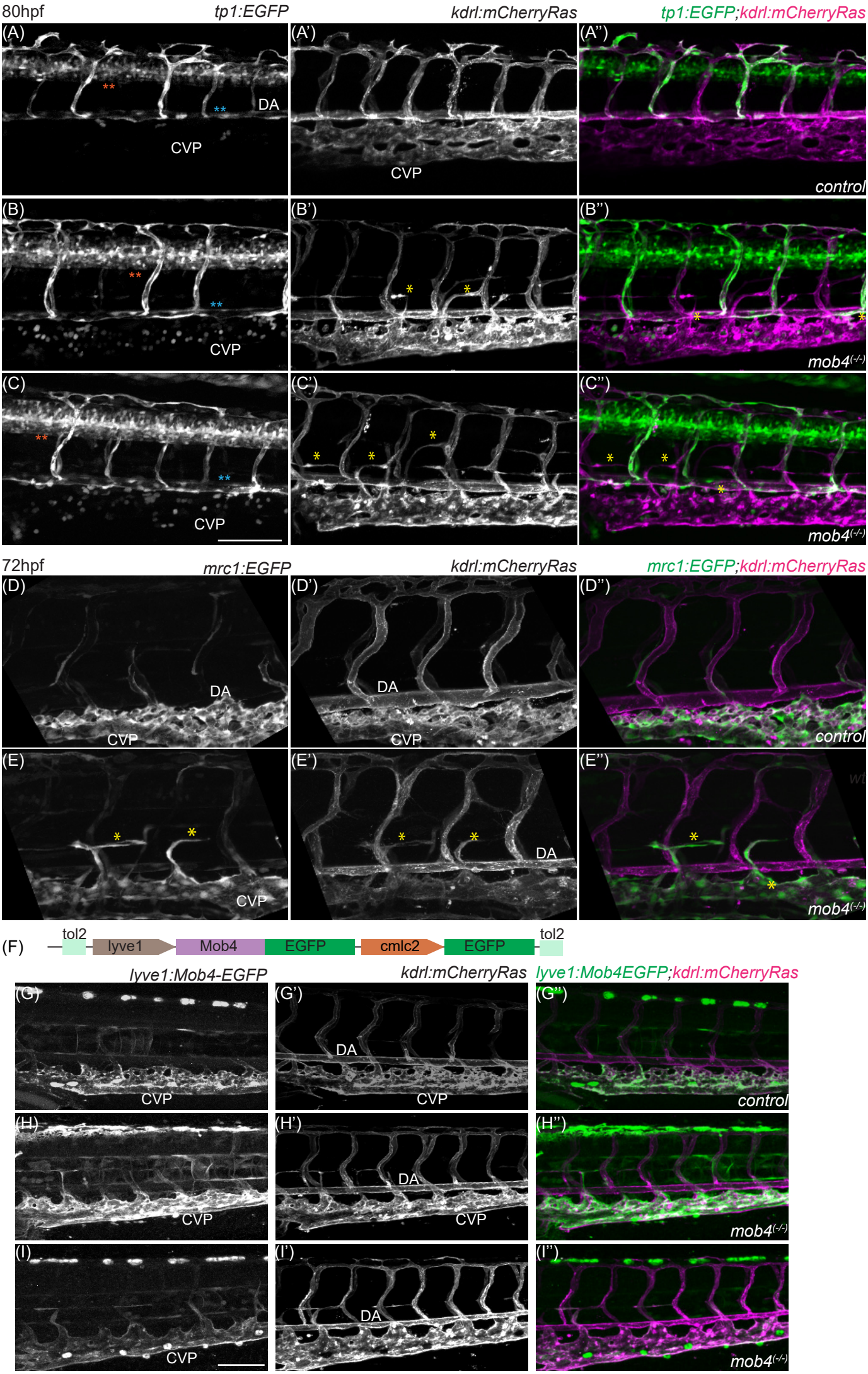
80hpf
tp1:EGFP
kdrl:mCherryRas
tp1:EGFP;kdrl:mCherryRas
(A)
(A')
(A'')
DA
CVP
control
(B)
(B')
(B'')
mob4(-/-)
(C)
(C')
(C'')
72hpf
mrc1:EGFP
kdrl:mCherryRas
mrc1:EGFP;kdrl:mCherryRas
(D)
(D')
(D'')
(E)
(E')
(E'')
(F)
tol2
lyve1
Mob4
EGFP
cmlc2
EGFP
tol2
lyve1:Mob4-EGFP
kdrl:mCherryRas
lyve1:Mob4EGFP;kdrl:mCherryRas
(G)
(G')
(G'')
(H)
(H')
(H'')
(I)
(I')
(I'')

**Figure 5**

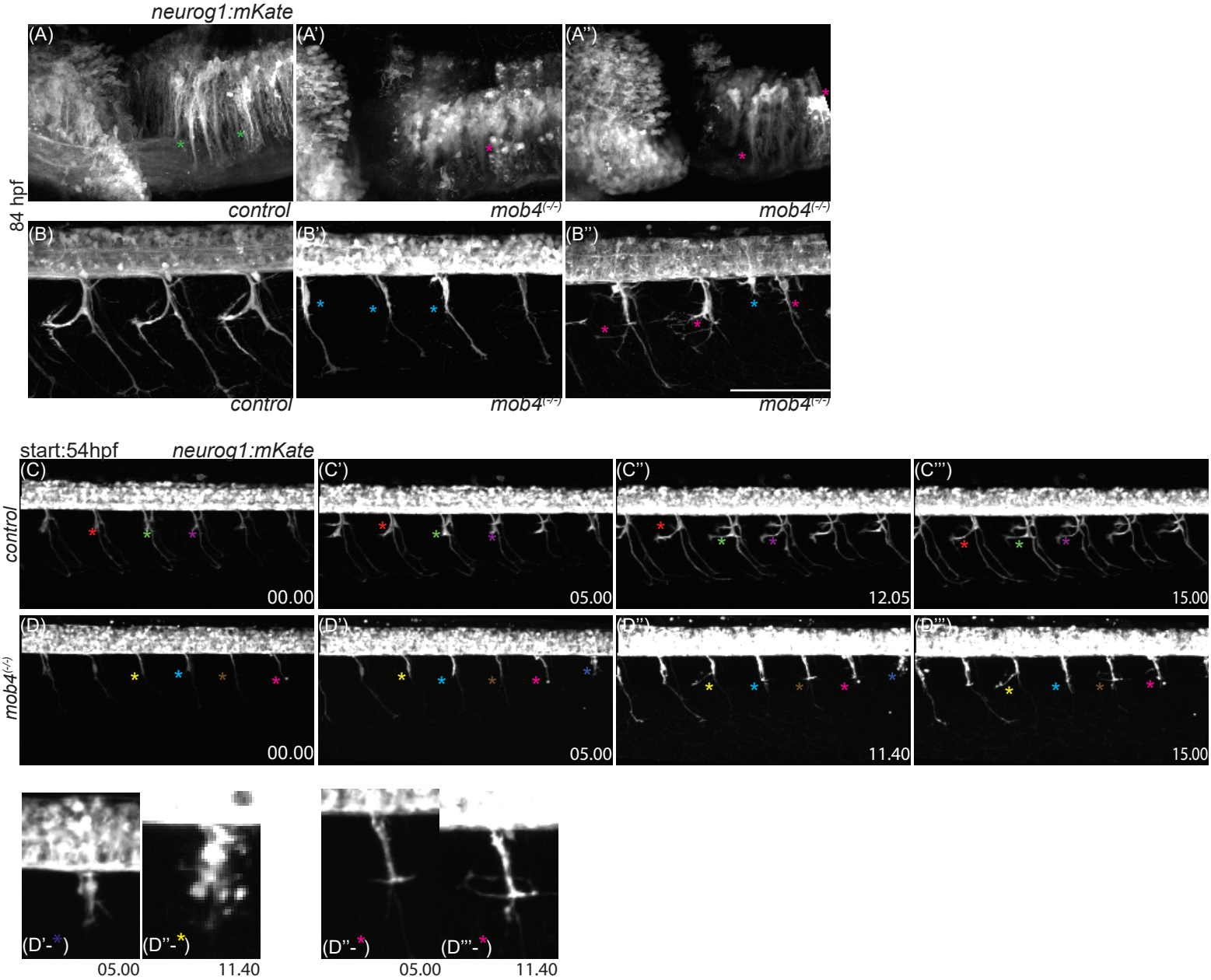
neurog1:mKate
(A)
(A')
(A'')
84 hpf
control
mob4(-/-)
mob4(-/-)
(B)
(B')
(B'')
control
mob4(-/-)
mob4(-/-)
start:54hpf
neurog1:mKate
(C)
(C')
(C'')
(C''')
control
00.00
05.00
12.05
15.00
(D)
(D')
(D'')
(D''')
mob4(-/-)
00.00
05.00
11.40
15.00
(D'-*)
(D''-*)
05.00
11.40
(D''-*)
(D'''-*)
05.00
11.40

Figure 6

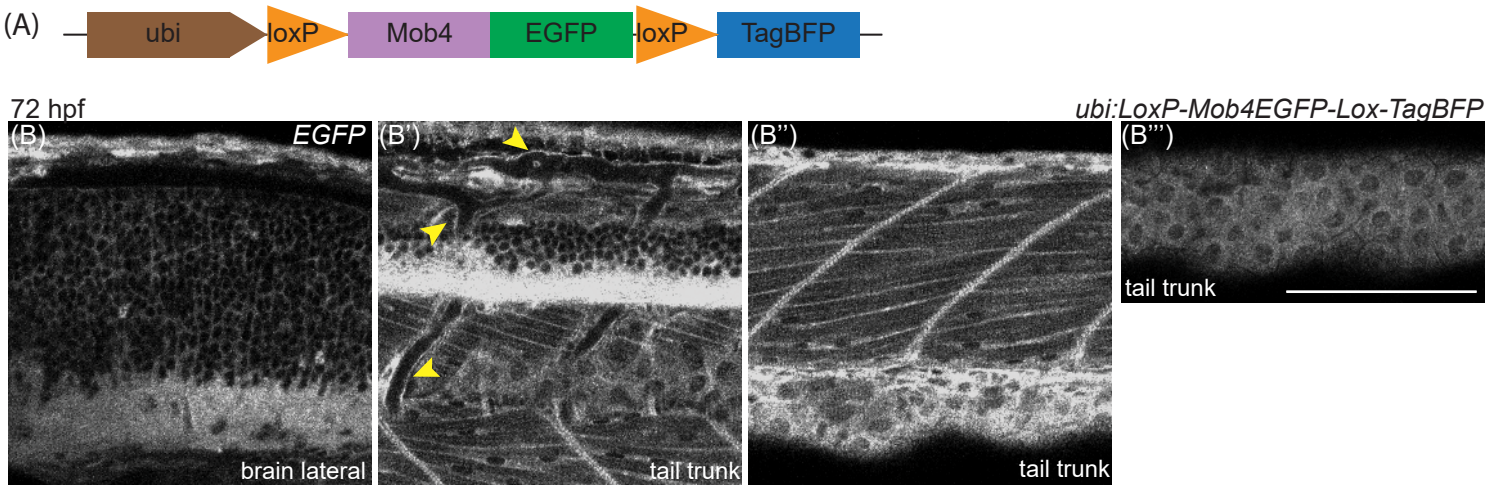


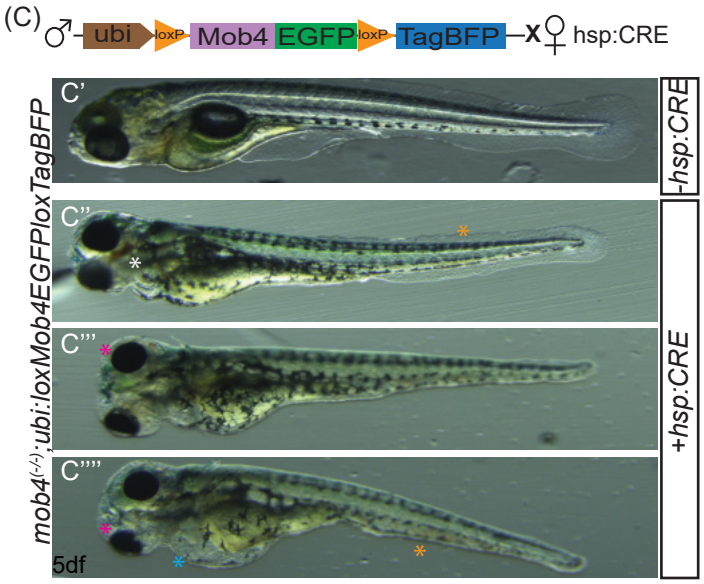


(D)

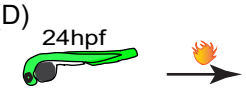


**Adult genotypes**

16/47: *mob4(-/-); ubi:loxMob4EGFPLoxTagBFP*
19/47:*mob4(+/-); ubi:loxMob4EGFPLoxTagBFP;hsp:Cre*
16/47:*mob4(+/-); ubi:loxMob4EGFPLoxTagBFP*
***0/47***: *mob4(-/-); ubi:loxMob4EGFPLoxTagBFP; hsp:Cre*

(D')

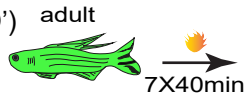


**lethality by 5 month post hs:**

*mob4(-/-);ubi:loxMob4EGFPLoxTagBFP; hsp:Cre:* 9/13
*mob4(+/-);ubi:loxMob4EGFPLoxTagBFP; hsp:Cre: 1/6*

(E) Vascular Mob4 lof

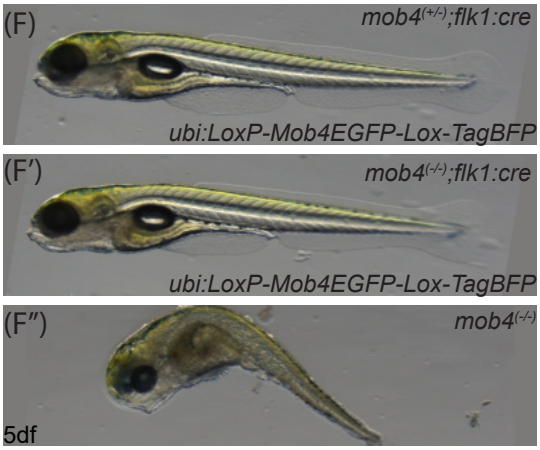


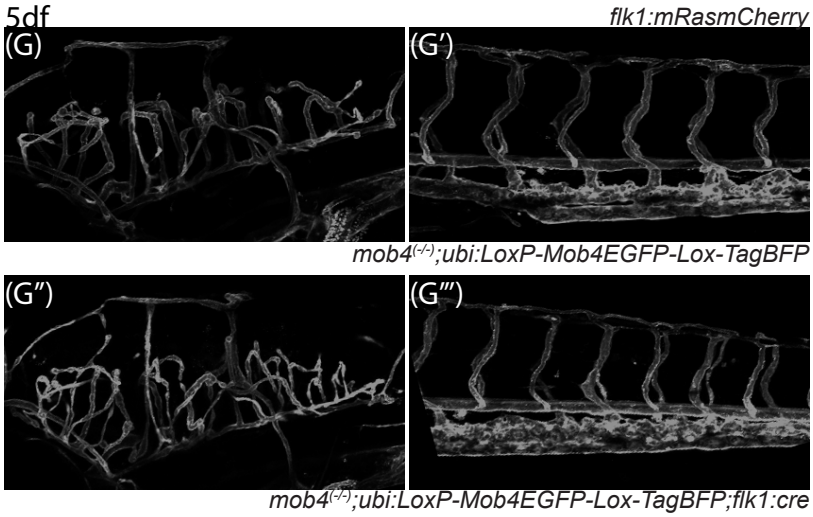


(H)

**Adult genotypes**

11/24 : *mob4(-/-); ubi:loxMob4EGFPLoxTagBFP*
3/11 : *mob4(-/-); ubi:loxMob4EGFPLoxTagBFP; flk1:Cre* *(vascular Mob4 lof)*

**Figure S1**

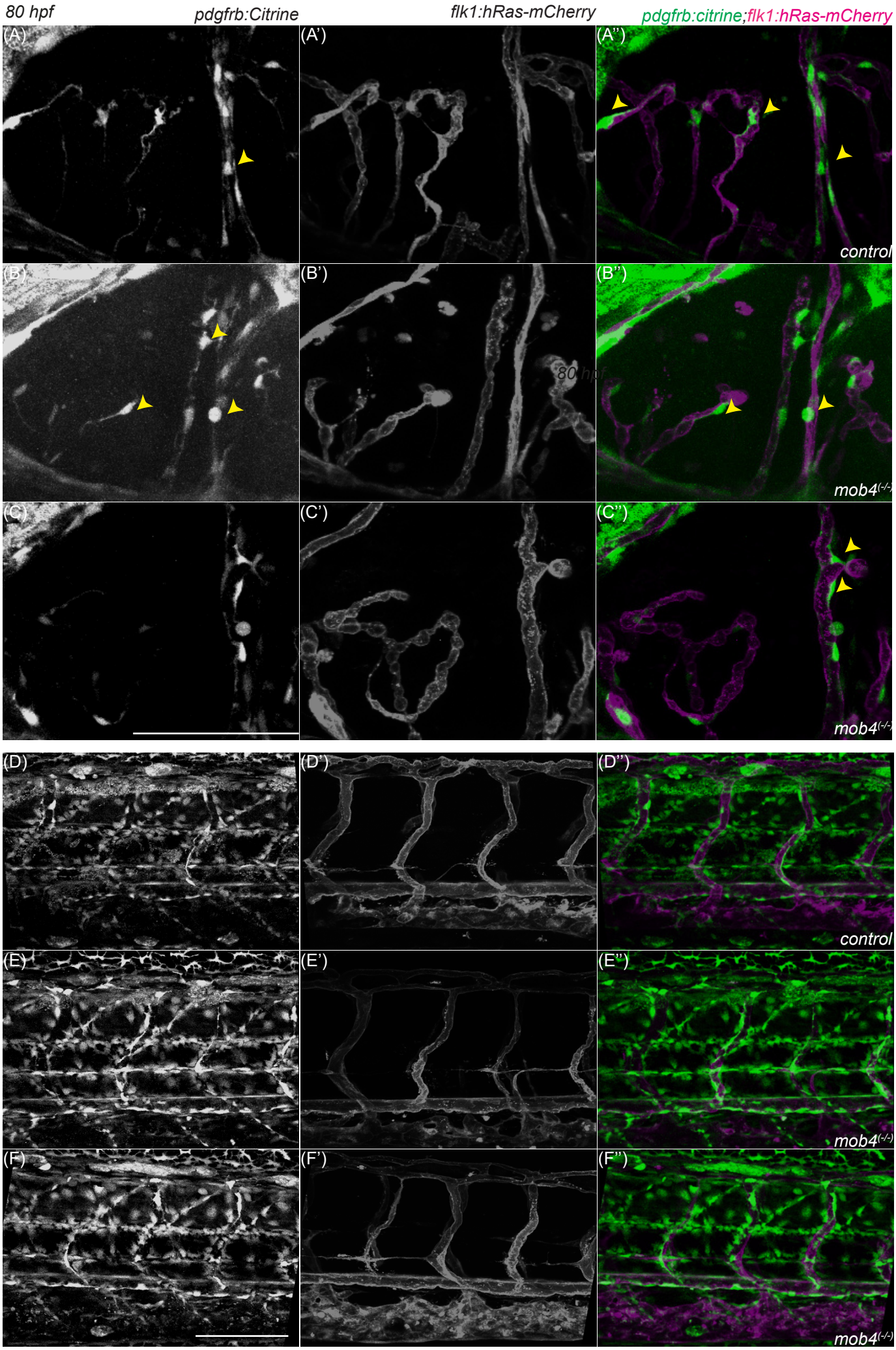
80 hpf
pdgfrb:Citrine
flk1:hRas-mCherry
pdgfrb:citrine;flk1:hRas-mCherry
(A)
(A')
(A'')
control
(B)
(B')
(B'')
80 hpf
mob4(-/-)
(C)
(C')
(C'')
mob4(-/-)
(D)
(D')
(D'')
control
(E)
(E')
(E'')
mob4(-/-)
(F)
(F')
(F'')
mob4(-/-)

**Figure S2**

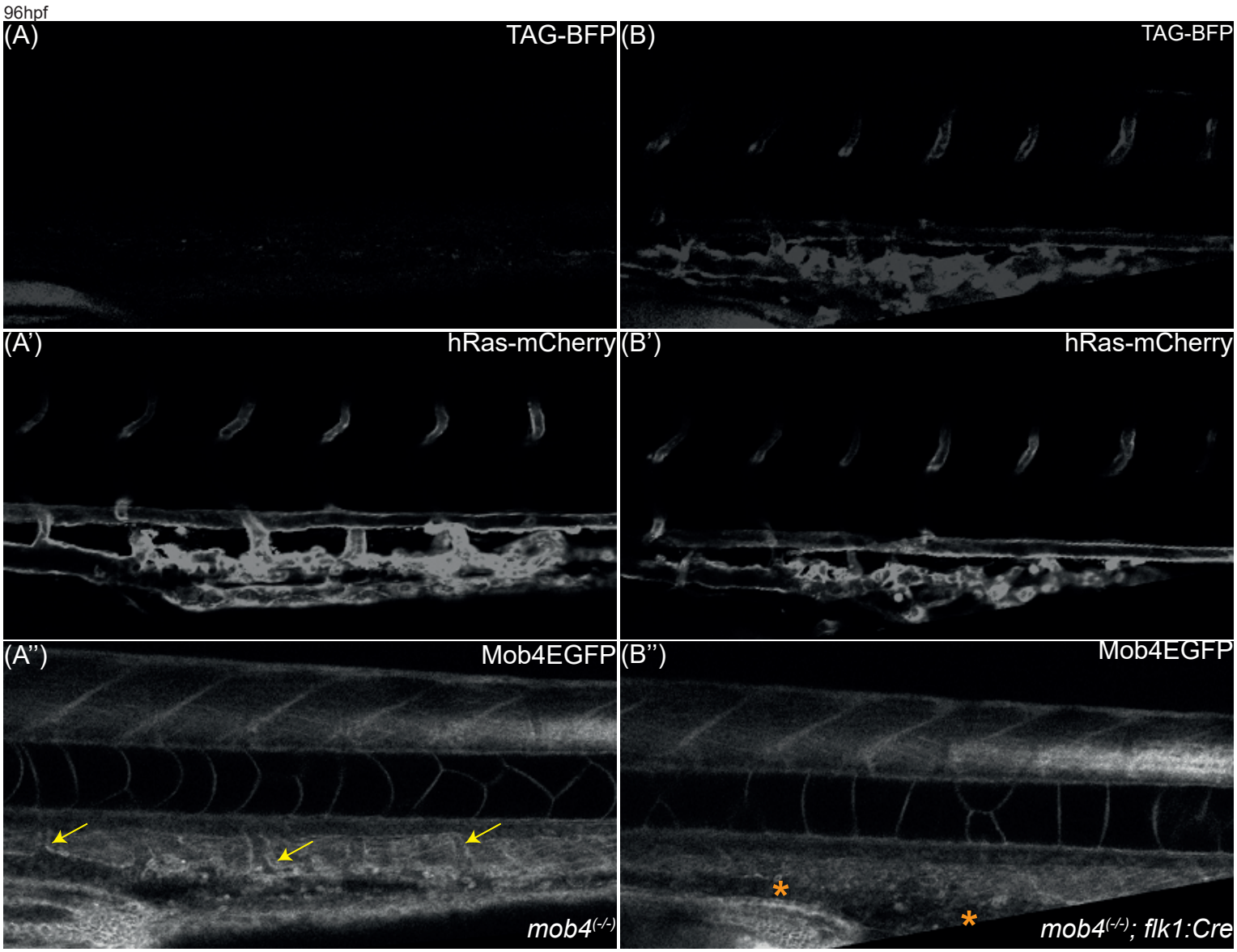
96hpf
(A)
TAG-BFP
(B)
TAG-BFP
(A')
hRas-mCherry
(B')
hRas-mCherry
(A'')
Mob4EGFP
mob4(-/-)
(B'')
Mob4EGFP
mob4(-/-); flk1:Cre

**Figure S3**

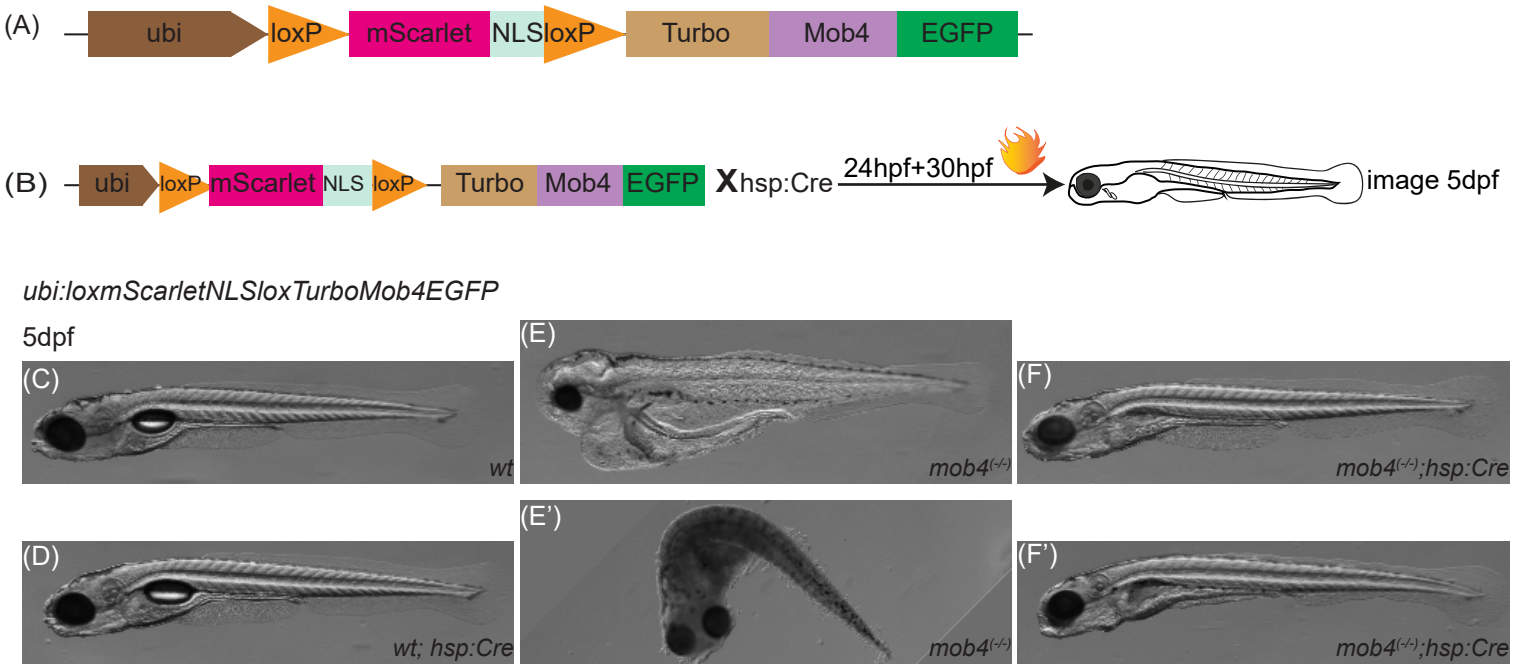
(A)
ubi
loxP
mScarlet
NLS
loxP
Turbo
Mob4
EGFP
(B)
ubi
loxP
mScarlet
NLS
loxP
Turbo
Mob4
EGFP
X hsp:Cre
24hpf+30hpf
image 5dpf
ubi:loxmScarletNLSloxTurboMob4EGFP
5dpf
(C)
wt
(E)
mob4(-/-)
(F)
mob4(-/-);hsp:Cre
(D)
wt; hsp:Cre
(E')
mob4(-/-)
(F')
mob4(-/-);hsp:Cre